# Improved Rate Capability and Thermal Stability of $LiNi_{0.5}Co_{0.2}Mn_{0.3}O_2$ Cathode Materials via Nanoscale $SiP_2O_7$ Coating

Yong-Seok Lee

Interdisciplinary School of Green Energy
Graduate School of UNIST

# Improved Rate Capability and Thermal Stability of $LiNi_{0.5}Co_{0.2}Mn_{0.3}O_2$ Cathode Materials via Nanoscale $SiP_2O_7$ Coating

A thesis
submitted to the Interdisciplinary School of Green Energy
and the Graduate School of UNIST
in partial fulfillment of the
requirements for the degree of
Master of Science

Yong-Seok Lee

12.21.2011
Approved by

Major Advisor
[Jaephil Cho]

# Improved Rate Capability and Thermal Stability of $LiNi_{0.5}Co_{0.2}Mn_{0.3}O_2$ Cathode Materials via Nanoscale $SiP_2O_7$ Coating

Yong-Seok Lee

This certifies that the thesis of Yong-Seok Lee is approved.

12.21.2011

[signature]

Thesis supervisor: [Jaephil Cho]

[signature]

[Hyun-Kon Song]

[signature]

[Kyu Tae Lee]

[signature]

[Yoon Seok Jung]

# Contents

# Abstract

In order to overcome the inherent problems of $LiNiO_2$, many method, such as coating and doping have been investigated. However, none of previous studies have not been reported to solve both rate capability at higher rates and thermal stability of the Ni-based cathode materials simultaneously. Here, we report the $Li_\delta P_y O_z$–coated $LiNi_{0.5}Co_{0.2}Mn_{0.3}O_2$ cathode materials doped with P and Si ions which possesses both higher rates and thermal stability. It was prepared by direction reaction of LiOH and $SiP_2O_7$-coated $Ni_{0.5}Co_{0.2}Mn_{0.3}(OH)_2$ precursors. The coated cathodes exhibited quite impressive results; rate capability was improved by almost 100% at a 7C rate compared to pristine $LiNi_{0.5}Co_{0.2}Mn_{0.3}O_2$. Furthermore, the amount of heat generation at 4.5V charge cut-off as a result of the evolution of oxygen was reduced by 79%, compared to pristine $LiNi_{0.5}Co_{0.2}Mn_{0.3}O_2$ sample. Overall, this coating method is also applicable to other bulk cathodes, such as $LiMn_2O_4$ and $LiCoO_2$ which need to improve electrochemical properties both at room and elevated temperatures.

# Figure captions

**Figure 1.** A schematic presentation of the most commonly used Li-ion battery based on graphite anodes and $LiMO_2$ cathodes.

**Figure 2.** Crystal structure of $LiMO_2$ having the O3 layered structure

**Figure 3**. a–) TEM images of the $MPO_4$ nanoparticles-coated $LiCoO_2$ bulk particle (10mm). e) Discharge capacities versus cycle number of $MPO_4$-coated $LiCoO_2$ in coin-type half cells. Adapted with permission from [72]. Copyright 2005 The Electrochemical Society.

**Figure 4**. a, b) SEM images of the uncoated and $TiO_2$-coated $LiCoO_2$ bulk particle (20mm; red dots are mapping of Ti element). c) Line mapping of Co and Ti elements along the line from surface to the inner part of the coated $LiCoO_2$ particles. d) Voltage profiles of the uncoated and coated $LiCoO_2$ cathodes at different C rates (0.2-1 and 0.2–10 denote first and tenth cycles at a rate of 0.2 C).

**Figure 5**. **(a)** Schematic views of the preparation procedure for the $SiP_2O_7$ coating on the cathode and (b) SEM images of $Ni_{0.5}Co_{0.2}Mn_{0.3}(OH)_2$ and annealed $Ni_{0.5}Co_{0.2}Mn_{0.3}O_2$ particles after $SiP_2O_7$ coating at 800°C for 16h.

**Figure 6**. (a) Power XRD pattern and (b) SEM image of as-prepared $SiP_2O_7$ nanoparticles.

**Figure 7**. Powder XRD profiles and the fitted profiles of (a) the pristine $LiNi_{0.5}Co_{0.2}Mn_{0.3}O_2$ (b) coated $LiNi_{0.5}Co_{0.2}Mn_{0.3}O_2$, respectively. Reliability factors (R-factor) obtained from the fitting are as follows: the pristine $LiNi_{0.5}Co_{0.2}Mn_{0.3}O_2$ : $R_p$ = 4.69, $R_{wp}$ = 6.70, $R_{exp}$ = 3.88; coated $LiNi_{0.5}Co_{0.2}Mn_{0.3}O_2$ : $R_p$ = 3.38, $R_{wp}$ = 4.95, $R_{exp}$ = 3.84, and (c) proposed structure of the coated cathode based upon the fitting.

**Figure 8**. Nano-SIMS of cross-sectioned coated $LiNi_{0.5}Co_{0.2}Mn_{0.3}O_2$ cathode particle (a: cross-sectioned image, b: mapping of lithium, c: mapping of P, and d: mapping of Si)

**Figure 9**. XPS of (a) Ni2p, (b) Co2p, and (c) Mn2p in the pristine and coated $LiNi_{0.5}Co_{0.2}Mn_{0.3}O_2$.

**Figure 10**. XPS of (a) $Si2p_{3/2}$ and (b) $P2p_{3/2}$ in the coated $LiNi_{0.5}Co_{0.2}Mn_{0.3}O_2$ and $SiP_2O_7$ nanoparticles.

**Figure 11**. (a and b) TEM images of the coated $LiNi_{0.5}Co_{0.2}Mn_{0.3}O_2$. (b) is high resolution TEM image of dotted area of (a) and digitalized Fourier-transformed images of red dotted areas of (b).

**Figure 12. (a)** Voltage profiles of pristine and coated $LiNi_{0.5}Co_{0.2}Mn_{0.3}O_2$ cathodes between 4.5 and 3V while increasing the C rate from 0.2 to 7C in lithium half cells (2016R type) at 21°C and (b) rate capability test of (a) from 0.2 to 7C rates. 1C was set at 185 $mAg^{-1}$ and charge and discharge rates are same and three identical coin-cells were used for pristine sample test.

**Figure 13**. Plots of working voltage (cell potential at a half value of the discharge or charge capacities) in the pristine and coated $LiNi_{0.5}Co_{0.2}Mn_{0.3}O_2$ with increasing C rates from 0.2 to 7C at 21°C.

**Figure 14**. Plot of discharge capacuty as a function of cycle number in lithium half cells containing pristine and coated $LiNi_{0.5}Co_{0.2}Mn_{0.3}O_2$ cathodes between 4.5 and 3V at 60°C. Cells were cycled at a

rate of 0.5C.

**Figure 15**. Nyquist plot Plots of the pristine and coated $LiNi_{0.5}Co_{0.2}Mn_{0.3}O_2$ before and after cycling at 60°C. Tables shows esiniated vlaues of $R_o$, $R_{SEI}$, and $R_{ct}$ using the equivalnet curcuit (top).

**Figure 16**. XPS of $Ni2p_{3/2}$ of pristine and coated $LiNi_{0.5}Co_{0.2}Mn_{0.3}O_2$ electrodes before and after cycling at 60°C (etching depths were 15, 30, and 60nm).

**Figure 17**. Plots of demension ratio of $Ni^{2+}$ and $Ni^{3+}$ peaks of **Figure 12**.

**Figure 18.** DSC scans of pristine and coated $Li_{0.1}Ni_{0.5}Co_{0.2}Mn_{0.3}O_2$ samples after charging at 4.5 V between 100°C and 350°C at a scan rate of 5°C/min.

**Figure 19**. In situ XRD patterns of (a) pristine and (b) coated $Li_{0.1}Ni_{0.5}Co_{0.2}Mn_{0.3}O_2$ electrode between 25°C and 325°C under sealed Ar chamber.

**Figure 20**. Evolution of the $c_{hex}/\ a_{hex}$ ratio as a function of temperature for pristine and coated cathodes.

---

## Table captions

**Table 1.** Rietveld refinement result of pristine $LiNi_{0.5}Co_{0.2}Mn_{0.3}O_2$ and coated $LiNi_{0.5}Co_{0.2}Mn_{0.3}O_2$ samples

# I. INTRODUCTION

$LiNiO_2$ materials have been in the spotlight as an alternative to $LiCoO_2$. Therefore, many methods, such as coating and doping, have been investigated to enhance the inherent problems of $LiNiO_2$. [1-14] Naturally unstable $Ni^{3+}$ ions are apt to reduce to $Ni^{2+}$ on the cathode surface in the form of NiO, and further structural instability from the higher oxidation state of $Ni^{4+}$ leads to substantial oxygen generation from the lattice at elevated temperatures. Particularly, the thermal instability problem leads to a faster thermal runway than $LiCoO_2$[15-18] and have demonstrated larger amounts of oxygen generation from the lattice with increasing charge cut-off voltage. Recently, larger amounts of Ni were substituted by electrochemical inactive Mn ions (e.g., $LiNi_{0.6}Co_xMn_{0.4-x}O_2$) to render such inherent problems [19-22], but increasing the Mn content increased the charge transfer resistance, resulting in decreased electrochemical performance (rate capability). On the contrary, increasing Mn content preserves initial structural integrity during the high-temperature heating as well as electrochemical cycling[23]. However, none of previous studies have not been reported to solve both rate capability at higher rates and thermal stability of the Ni-based cathode materials simultaneously.

In this regard, coating on the cathode material may lead to solve both rate capability and thermal instability upon delithiated states. However, previous coating method on Ni-based cathode materials led to improve either thermal stability or cycling performance, for example via dry $TiO_2$[10] or $SiO_2$[12] coatings. Alternatively, we can consider $AlPO_4$ coating [24], but this coating method due to usage of acidic coating solution led to partial dissolution of Li from the cathode material, in turn, increasing gas evolution at elevated temperatures.

In this study, we report that direction reaction of LiOH and $SiP_2O_7$-coated $Ni_{0.5}Co_{0.2}Mn_{0.3}(OH)_2$ particles leads to the simultaneous formation of an amorphous $Li_\delta P_yO_z$–like coating layer and a solid solution $LiNi_{0.5}Co_{0.2}Mn_{0.3}O_2$with doped Si and P ions. This new cathode material exhibitsignificantly improved rate capability and suppressed oxygen evolution the lattice at 4.5V above 200°C, compared to the pristine sample.

# II. REVIEW OF RELATIVE LITERATURE

## 2.1 Introduction to Li-ion batteries

Primary Li batteries became a commercial reality during the 1970s. Their categorization and characterization are well described in numerous books and hundreds of publications.[25-28] attempts to develop rechargeable Li batteries with Li-metal anodes have accompanied the R&D of Li batteries from their early stages. However, a few nearly commercial products of secondary Li (metal) batteries appeared during the early 1990s. These included Li–TiS2,[29] Li–MoS2[30] and Li–$Li_xMnO_2$ systems[31] The last system, developed by Tadiran Inc. (Israel) in the mid 1990s, was a commercial AA battery that was addressed to power cellular phones. Li–$MoS_2$ and Li–$TiS_2$ systems did not take off due to safety problems. The Li–LixMnO2 system, which was considered to be safe (due to the included internal safety mechanisms),[32] failed due to the prolonged time required for charging Li metal-based batteries in order to obtain prolonged cycle life (several hours per cycle).[33] From the early stages of R&D of Li-ion batteries, it was clear that transition metal oxides and sulfides can serve as excellent reversible cathode materials for rechargeable Li batteries.[25, 26] The Li-ion battery technology evolution, which enabled the commercialization of the rechargeable, high energy density batteries that are conquering the market, emerged due to the introduction of graphite as the anode material instead of Li metal, and the use of lithiated transition metal oxide cathode materials: $LiMO_2$ as the source of lithium in the cell.[34] Graphite–$LiMO_2$ became the leading Li-ion battery system that at present powers most of the portable electronic devices: cellular phone, laptops, digital cameras, etc. Fig. 1 illustrates the basic Li-ion battery system that leads the current battery market, and serves as the starting point for the following review.

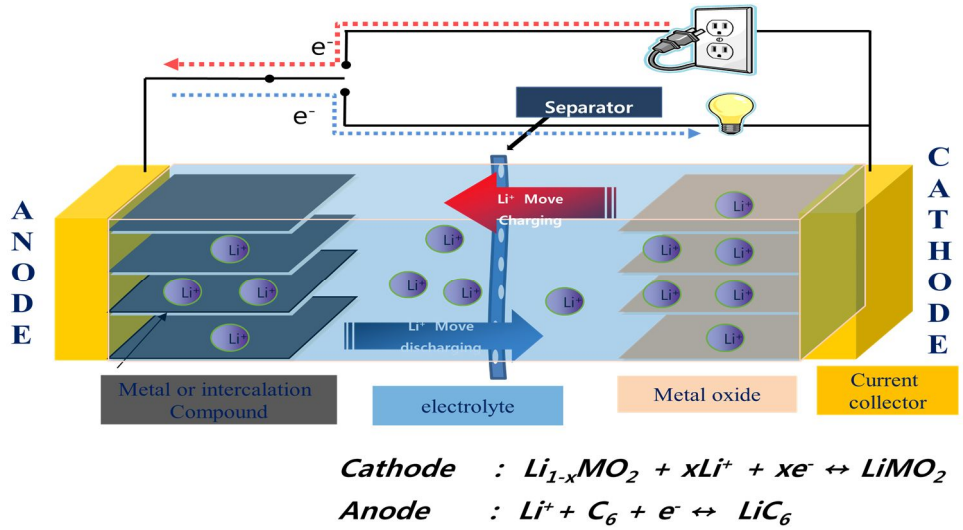


**Figuer 1.** A schematic presentation of the most commonly used Li-ion battery based on graphite anodes and $LiMO_2$ cathodes.

The main cell reactions are reversible Li-ion intercalation-de-intercalation cycles between two layered compounds. In order to ensure the anodic stability of both the cathode material and the electrolyte solutions, the cathode reactions are:

$Li_{1-x}MO_2 + xLi^+ + xe^- \leftrightarrow LiMO_2$

The upper potential of the delithiation of $LiCoO_2$ is limited to 4.2 V (vs. Li/Li+), which means that only half of the theoretical capacity of the cathode, around 140 mAh g_1 is extracted in a reaction that is mainly first-order phase transition between $LiCoO_2$ and $Li_{0.5}CoO_2$.[35] As mentioned above, the source of lithium in these Li-ion batteries is the cathode material, which ensures a very prolonged shelf life and excellent safety features, compared to Li metal-based batteries. The first process in the cell is always charging, namely, oxidation and delithiation of $LiCoO_2$ in parallel to the reduction and lithiation of graphite. Graphite intercalates reversibly with lithium to form LiC6 as the final product according to the following reaction:

$Li^+ + C_6 + e^- \leftrightarrow LiC_6$

The intercalation of Li into graphite occurs in stages such as $LiC_{24}$, $LiC_{27}$ and $LiC1_2$ via first-order phase transition reactions between the various stages.[36] A first polarization of graphite electrodes in any polar aprotic Li salt solution consumes irreversible charge, for the reduction of solution species. These processes, as will be discussed later, may form passivating films that prevent any further irreversible process and provide metastable conditions for the $Li_xC_6$ stages that are formed during the course of Li insertion into graphite, all of which are highly reducing agents,[37] Hence, each Li-ion battery has to contain the Li source, namely, the cathode material ($Li_xMO_2$) in excess, in order to provide the Li ions and the charge that is needed to form the passivating surface films on graphite. A critical engineering task in the development of practical Li-ion batteries is to reduce to a minimum the above reversible charge consumption and hence, the extra content of the cathode material.

### 2. 1. 1 Layered oxide cathodes

Several oxides with a general formula $LiMO_2$(M=V, Cr, Co, and Ni) crystallize in a layered structure in which the $Li^+$ and $M^{3+}$ ions occupy the alternate (111) planes of the rock salt structure to give a layer sequence of O-Li-O-M-O along the c axis as shown in Figure 1 for $LiCoO_2$. The structure has an oxygen stacking sequence of ABCABC along the c axis and the $Li^+$ and $M^{3+}$ ions occupy the octahedral interstitial sites of the cubic close-packed oxygen array. This structure is designated as the O3 layer structure since the $Li^+$ ions occupy the octahedral sites (O referring to octahedral) and there are three $MO_2$ sheets per unit cell. The structure with a strongly (covalently) bonded $MO_2$ layers allows a reversible extraction/insertion of lithium ions from/into the lithium planes. The interconnected lithium-ion sites through the edge-shared $LiO_6$ octahedral arrangement between the

$MO_2$ layers provide fast two-dimensional lithium ion diffusion leading to high $\sigma_{Li}$, On the ather hand, the edge-shared $MO_6$ octahedral arrangement with a direct M-M interaction can provide good electronic conductivity $\sigma_c$ depending on the electronic configuration of the $M^{3+}$ ion. As a result, the $LiMO_2$ oxides crystallizing in the O3 structure have become attractive candidates as cathodes.

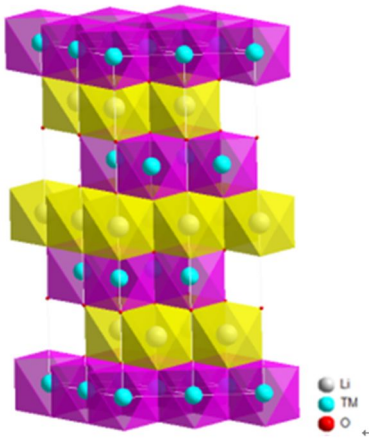


**Figure 2.** crystal structure of $LiMO_2$ having the O3 layered structure

### 2.1.1.1 $LiNiO_2$

Lithium nickel oxide is same structural with lithium cobalt oxide structure but has not been pursued in the pure state as Li-ion battery cathode material for a variety of reasons, Although nickel is readily available compared to cobalt. First, it is difficult that stoichiometric $LiNiO_2$ exists. Most of the reports suggest excess nickel as in $Li_{1-y}Ni_{1+y}O_2$; thus, nickel is as often as found in the lithium layer, which is fixed with the $NiO_2$ layers, there are controlled by reducing the lithium diffusion coefficient and the power capability of the electrode. Second, compounds appear to be unstable together low lithium contents because of the high effective equilibrium oxygen partial pressure, so such cells are inherently unstable and dangerous in contact with electrolyte. A secondary lithium can be inserted either chemically or electrochemically in $Li_{1.8}Ni_{1+y}O_2$, which is a mixture as expected of "$LiNiO_2$"and "$Li_2NiO_2$".[38] The former assists in ordering the structure, that is keeping the nickel in the nickel layer, and the latter, being redox inactive, prevents the complete removal of all the lithium, thus additionally stabilizing the structure and preventing any phase changes that might occur at very low or zero lithium content.

### 2.1.1.2 $LiNi_{1-y}Co_yO_2$

Many different candidates can be substituted into the layered structure, and they impact the layeredness structure, its stability on lithium removal, and the capacity retention for cycling. In a series of papers the Delmas group [39-42] determined by the physical properties and structural details of the $LiNi_{1-y}Co_yO_2$ and indicated that there is an increased ordering as the cobalt concentration increases; they found that the $c/3a$ ratio increases monotonically from 1.643 to 1.652 as $y$ increases from 0 to 0.4 and that there is no nickel content on the lithium sites for $y$ g 0.3. Thus, cobalt suppresses the migration of nickel to the lithium site in the mixed Li nickel/cobalt compounds and one would expect and finds the same behavior in the Li nickel/manganese/cobalt oxides. Cobalt is also reported to facilitate the oxidation of iron atoms in the structure.[43] Other ions, such as iron, do not have the same positive effect as cobalt; thus, in the compound $LiNi_{1-y}Fe_yO2$ the capacity is reduced with increasing iron content and the iron has no positive effects on the layeredness of the structure.[44] Thus, for $y$ ) 0.10, 0.20, and 0.30 the amount of 3d metal in the lithium layer is 6.1%, 8.4%, and 7.4%, respectively, for samples formed at 750 °C. Although a LiFeO2 compound would be ideal for a low-cost battery, it has been reported[45] that the lithium cannot be deintercalated within the normal potential ranges used in lithium batteries; this is explained174 by the lack of compression of the $FeO_6$ octahedra which makes the reduction of one electron from $Fe^{3+}$ very difficult. An issue with all these layered oxides is their electronic conductivity, which is not uniformly high across the lithium composition range, or nickel substitution. Thus, cobalt substitution in $LiNiO_2$, as in $LiNi_{0.8}Co_{0.2}O_2$, reduces the conductivity.[42] In addition, as lithium is removed from the phase $Li_xNi_{0.1}Co_{0.9}O_2$[40] or from $LixCoO_2$ the conductivity was found to increase dramatically by some 6 orders of magnitude to around 1 S/cm from $x$ ) 1 to 0.6. These dramatic changes demand that a conductive diluent be added to the cathode-active material, which reduces both the energy storage and the power capabilities. Studies have shown that the cobalt-substituted nickel oxides are more stable and thus are less likely to lose oxygen than the pure nickel oxide. The addition of a little of a redox-inactive element such as magnesium reduces the capacity fading on cycling, [46] as in $LiNi_{1-y}Mg_yO_2$;[47] this inert element prevents the complete removal of all the lithium and thus minimizes possibly structural collapse and reaching such a high level of oxygen partial pressure- $NiO_2$ itself is thermodynamically unstable at 25 °C, as the equilibrium oxygen partial pressure exceeds 1 atm. Substituted nickel oxides, such as $LiNi_{1-y-z}Co_yAl_zO_2$, are prime candidates for the cathode of advanced lithium batteries for use in large-scale systems as required for hybrid electric vehicles. On charging these mixed oxides the nickel is oxidized first to Ni4+ then the cobalt to $Co^{4+}$.[42] SAFT has constructed cells with these substituted nickel oxides that have been cycled 1000 times at 80% depth of discharge with an energy density of 120-130 Wh/kg.[48]

### 2.1.1.3 $LiNi_{1-x-y}Co_xMn_yO_2$

Extensive research efforts have focused on other layered materials with reduced cobalt content, such as $LiNi_xCo_{1-x}O2$,[42] $LiNi_xCo_{1-2x}Mn_xO_2$,[49-51] and $LiNi_{1-x-y}Co_xMn_yO_2$.[52, 4, 53-55] Among them, Ni-rich material $LiNi_{1-x-y}Co_xMn_yO_2$ ($1 - x - y \_ 0.5$) has received much attention motivated by the promising performance of $LiNi_{1/3}Co_{1/3}Mn_{1/3}O_2$.[4, 54, 55] $LiNi_{1-x-y}Co_xMn_yO_2$ (Ni _ 0.5)-type cathode materials possess higher capacities than $LiNi_{1/3}Co_{1/3}Mn_{1/3}O_2$ due to their relatively higher content of Ni, which is the active redox species in the host structure. [4, 54, 55] $LiNi_{1-x-y}Co_xMn_yO_2$ (Ni ~ 0.5)-type layered cathode materials with various compositions of cobalt and manganese have different electrochemical behaviors as well as structural stabilities. The optimum compositions of metal ions for high capacity with acceptable stability is not yet clearly understood because an increase in the amount of Ni usually results in poor cycling performance as well as structural instability.[4, 56] Many studies have been carried out where the Ni content in Ni-rich materials has been varied, as well as the contents of other metals (e.g., Co and Mn).[4, 55, 57] However, thermal instability and gradual structural deformation over long-term cycling is still an obstacle for commercialization in Li-ion battery applications.[58, 59] Thermal instability as well as structural instability is usually caused by exothermic reactions of $LiNi_{1-x-y}Co_xMn_yO_2$ ($x + y \sim 0.5$) electrodes in the presence of electrolyte, accompanied by oxygen release from the host structure at an elevated temperature (55°C).[58-60] To stabilize the structural integrity of Ni-rich layered materials without sacrificing deliverable capacity, combinational substitutions with various cations have been studied.[61-64] The intrinsic properties of $LiNi_{1-x-y}Co_xMn_yO_2$-type materials strongly depends on the amounts of each metal ion (Ni, Co, Mn) mainly due to interactions between metal ions and the modification of M–O bonding.[65] In an effort to increase the energy density of electrode material while maintaining structural and electrochemical stability, it is necessary to find the optimal composition of the metal ions. By understanding the exact roles of Ni, Co, and Mn on the electrochemical properties, structural stability, and thermal stability of $LiNi_{1-x-y}Co_xMn_yO_2$, an improved design for high-performance Li-ion batteries is achievable.

### 2.1.2 Coating effect

Recent increase in the mobile electronics market has led to the rapid expansion in the demand for Li batteries. Since the discovery of the usefulness of layered $LiCoO_2$ in Li-ion cells, a number of electrode materials have been investigated on the cathode part because the cathode among the Li-ion cell assembly is the most important part, determining the cell capacity and safety. Many cathode materials with higher capacity and voltage well over $LiCoO_2$ have been intensively investigated. In spite of advanced electrochemical properties of enormous cathode derivatives, however, representative $LiCoO_2$ is currently still the most widely used material in the actual application. The main obstacles of bulk derivatives include dissolution of electrochemically active metal ion during the charge, thermal stability, and safety for overcharge. The slow diffusion rate of Li ion should be also enhanced for faster charge. These disadvantages of bulk-scale material can be anticipated to be overcome through nanoscale engineering and nanochemistry such as surface-coating and control of particle sizes and morphologies. Because the electrochemical reactions start at the electrode–electrolyte interface, control of the interfaces via coating can decrease the interface side reactions with the electrolyte and improve the Li-ion diffusivity. In addition, coating can lead to the decreased exothermic reaction of the delithiated cathode with electrolyte above 200°C. Although, a cathode material with a larger powder size has larger thermal stability upon charging, the rate capability and cycle-life performance deteriorate at a higher current rate. Considering these facts, recent research of cathode materials has concentrated on a surface modification by nanoscale coating and synthesis of well-designed nanoparticles with zero-, one- and two-dimensional morphologies. It can be anticipated that the formation of a nanoscale coating layer with thermal stability can provide higher electrode–electrolyte contact areas as well as more facile intercalation for Li ions. A series of metal oxide (Al2O3, ZrO2, TiO2, etc.) coating has been reported to be effective in overcoming these electrochemical shortcomings.[66] At the same time, one of the fastest growing research fields in cathode materials is nanochemical synthesis of cathodes with various morphologies. Under the circumstance of the saturation of bulk chemical composition change, dimension control can look forward to deriving much better electrochemical properties compared to those of corresponding bulk materials. In this regard, surface structural characterization should be followed since the nanostructured material itself has an intrinsic high surface-to-volume ratio. The Li-ion kinetics on the surface are quite different to that of the bulk. For example, a structural incompatibility between bulk and surface structures can be observed in the bulk $LiCo_{1/3}Ni_{1/3}$ $Mn_{1/3}O_2$ cathode through bulk-sensitive transition metal K-edge XAFS and surface-sensitive L-edge XAS.[67] During delithiation, electronic structural variations for each metal ion in the surface region are different to those of the bulk in the charge compensation process for the Li-ion behavior. Therefore, surface-sensitive spectroscopic

characterization is essential for nanostructured cathode materials. Nevertheless, the spectral technique has been rarely applied to nanostructured cathode materials. In future, this spectroscopic approach could lead to a breakthrough in the advancement of nanostructured cathodes, through the revelation of the relationship between electrochemical and surface-focused structural properties during Li-ion behavior.

#### 2.1.2.1 Nanoscale Coatings on Bulk Cathodes

One of the critical test items of the cathode material is the capability of storing charged states above 60°C. Highly oxidized transition metal ions in the charged $Li_xMO_2$ (M¼Co, Ni, and Mn) are apt to decompose electrolytes in the particle surface, resulting in substantial amounts of gas generation. In addition, it can be expected that metal-ion dissolution at elevated temperatures induces a simultaneous Li-ion dissolution from the cathode surface, accompanied by a structural degradation. Among the cathode materials, spinel $LiMn_2O_4$ has the most destabilized structure at elevated temperatures.[68-72] Self-discharge occurs during storage above 55°C and drastically affects cathode performance due to electrolyte decomposition at high voltages catalyzed by the electrode surface. Also, capacity fade upon cycling largely depends on Mn dissolution through the following reaction, $Mn_{3þ}$,$Mn_{4þ}$,$Mn_{2þ}$ (with $Mn_{2þ}$ going into the solution), which occurs in presence of trace acids, especially HF.[69, 70] A solution to this problem is to trap HF by means of a coating layer as HF scavenger as soon as it has been formed. The formation of such an inorganic passivation layer provides a twofold benefit in that it reduces disproportion–dissolution reactions and also minimizes electrolyte decomposition on the surface of the spinel. The first study on the cathode coating reported that $Al_2O_3$, $B_2O_3$, and $SiO_2$ coating on spinel $LiMn_2O_4$ can suppress Mn dissolution from $LiMn_2O_4$ at elevated temperatures.[73] However, the irreversible capacity and capacity retention of the coated sample are inferior to the bare sample despite the lower Mn dissolution rate at 55°C storage. Such deteriorated behavior of the coated cathode may be associated with the formation of a thick coating layer that impedes an easy Li-ion diffusion. Although the electrochemically inactive coating layer prevents the transition metal ion from dissolving to electrolyte, it can act as a resistance against Li-ion diffusion into the bulk. To overcome these problems, electrochemically active $LiCoO_2$, which allows Li-ion diffusion and has a strong resistance to HF, has been coated on the $LiMn_2O_4$ and shows improved capacity retention and lower irreversible capacity during cycling at 55°C.[74] $LiMn_2O_4$ has been also coated on $LiCoO_2$ to improve the thermal stability of the delithated $Li_xCoO_2$.[75] On the other hand, MgO, $SnO_2$, $Al_2O_3$, ZnO, $ZrO_2$, and $TiO_2$ coatings on layered $LiCoO_2$ and $LiNi_{1-x}M_xO_2$ via the sol–gel method have been intensively investigated.[75-78, 66, 3, 79-82, 2, 83-86] Among these coating materials, $ZrO_2$ coating exhibits the best capacity retention at >4.5 V cycling and high temperature storage at 90°C.[87] This

finding can be supported with the $ZrO_2$ coating on spinel $LiMn_2O_4$, which shows the lowest capacity fading at 55°C cycling among the various coating materials.[85] The improvement is due to the fact that $ZrO_2$ behaves as an effective HF scavenger. However, one of the drawbacks of the sol–gel-driven coating is that it is difficult to control the coating thickness. Simultaneously, the coating-layer materials should have a dual contribution to both tolerance for Li-ion diffusion and hindrance of dissolution of transition metal ion during the lithiation. In this regard, metal phosphate ($MPO_4$) coating is feasible to control the coating thickness where the uniformity and thickness of coating layer depends on the nature of M ion (Al, Fe, Ce, and SrH).[87, 88] Figure 3 shows that the $FePO_4$-coated $LiCoO_2$ shows a completely covered coating layer with a thickness of 25–50 nm, which is thicker than the $AlPO_4$-coated $LiCoO_2$. This is due to the larger $FePO_4$ particles than $AlPO_4$, even though the same coating concentration of ~ 1wt%has been used. In the case of $CePO_4$ and $SrHPO_4$, only a portion of the $LiCoO_2$ can be covered with the particles. However, it is interesting to note that the original whisker-type particle morphology of the $CePO_4$ is completely changed into an aggregation of 30–40-nm-sized particles.[88] The discharge capacities of the completely encapsulated $FePO_4$- and $AlPO_4$-coated $LiCoO_2$ show the highest discharge capacity, 230 mAh/g, and the $LiCoO_2$ cathodes with partially covered with $SrHPO_4$ and $CePO_4$ show~210 mAh/g. For example, the amount of Co dissolution after the first cycling increased in the order of bare (1053 ppm)>SrH ~ Ce (230 and 210 ppm) >Fe ~ Al (50 and 40 ppm, respectively). However, bare sample showed the smallest capacity of 190 mAh/g. This clearly indicates that the degree of coverage greatly affects the discharge capacity, and a complete covering was reported to be reduced the Co dissolution or any side reactions between the particle surface and electrolytes at higher cut-off voltages. In contrast to the conventional coating method using solvents, dry-coating is reported in the present study for the first time. The advantage of this method is simplifying a coating procedure and cost-saving in the coating processing. At first, $TiO_2$ nanoparticles with sizes below 100nm are mixed with $LiCoO_2$ particles with an average particle size of 20 mm in a rotating jar at 200 rpm. The mixed particles are then fired at 1000°C for 5 h in air.

Figure 4 shows scanning electron microscopy (SEM) images of the uncoated and 0.5 wt% $TiO_2$ nanoparticle coated $LiCoO_2$ cathode particles, which show quite similar surface morphologies to each other. In spite of using dry coating, Ti atoms appear to distribute uniformly throughout the particles. The line mapping of the Ti atoms across the cross-sectioned coated particle confirms that Ti atoms diffuse into the bulk particle. This result indicates that the thermal annealing of the $TiO_2$ nanoparticles on the bulk $LiCoO_2$ leads to the formation of $LiCo_{1-x}Ti_xO_2$ solid solution with higher Ti-atom concentration near the surfaces. These results indicate that dry coating can provide electrochemical results comparable to wet coatings reported previously. [11]

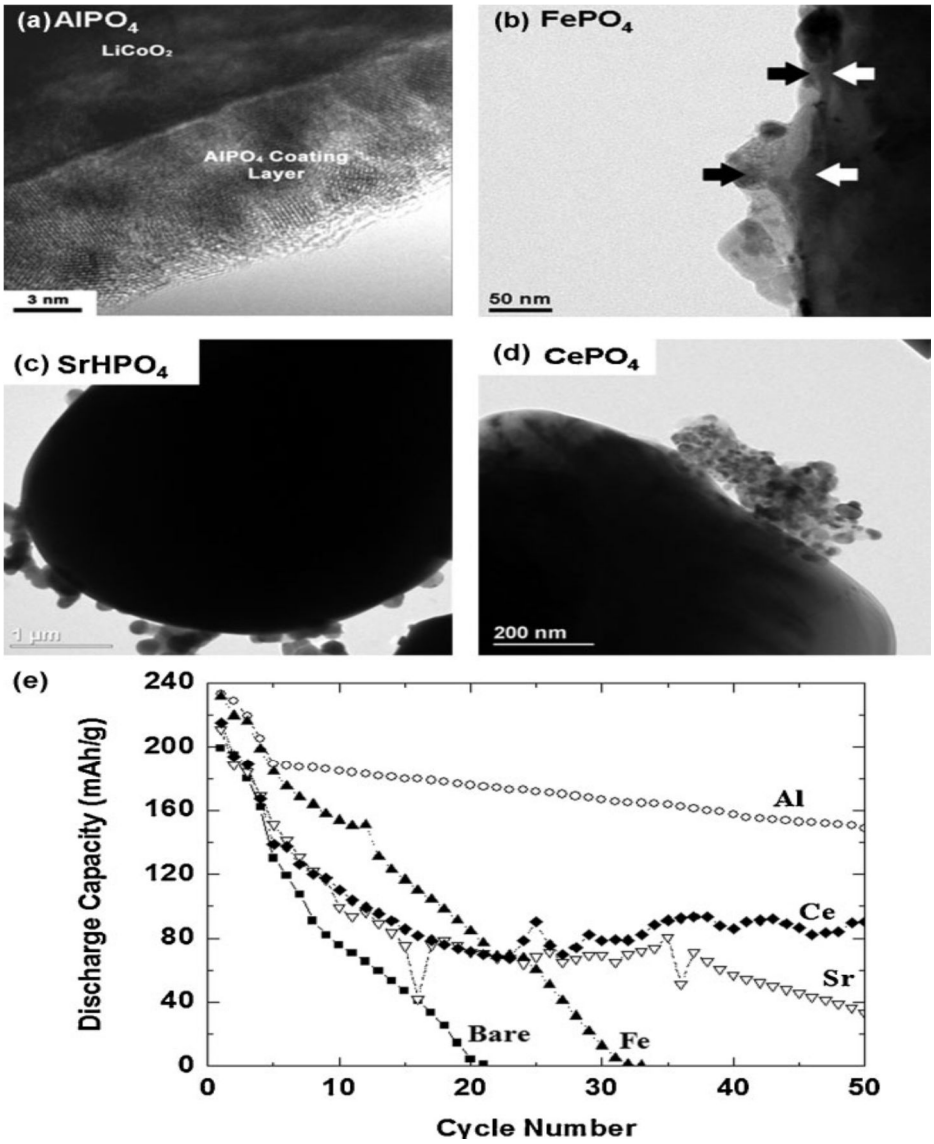


**Figure 3**. a–) TEM images of the $MPO_4$ nanoparticles-coated $LiCoO_2$ bulk particle (10mm). e) Discharge capacities versus cycle number of $MPO_4$-coated $LiCoO_2$ in coin-type half cells. Adapted with permission from [89]. Copyright 2005 The Electrochemical Society.

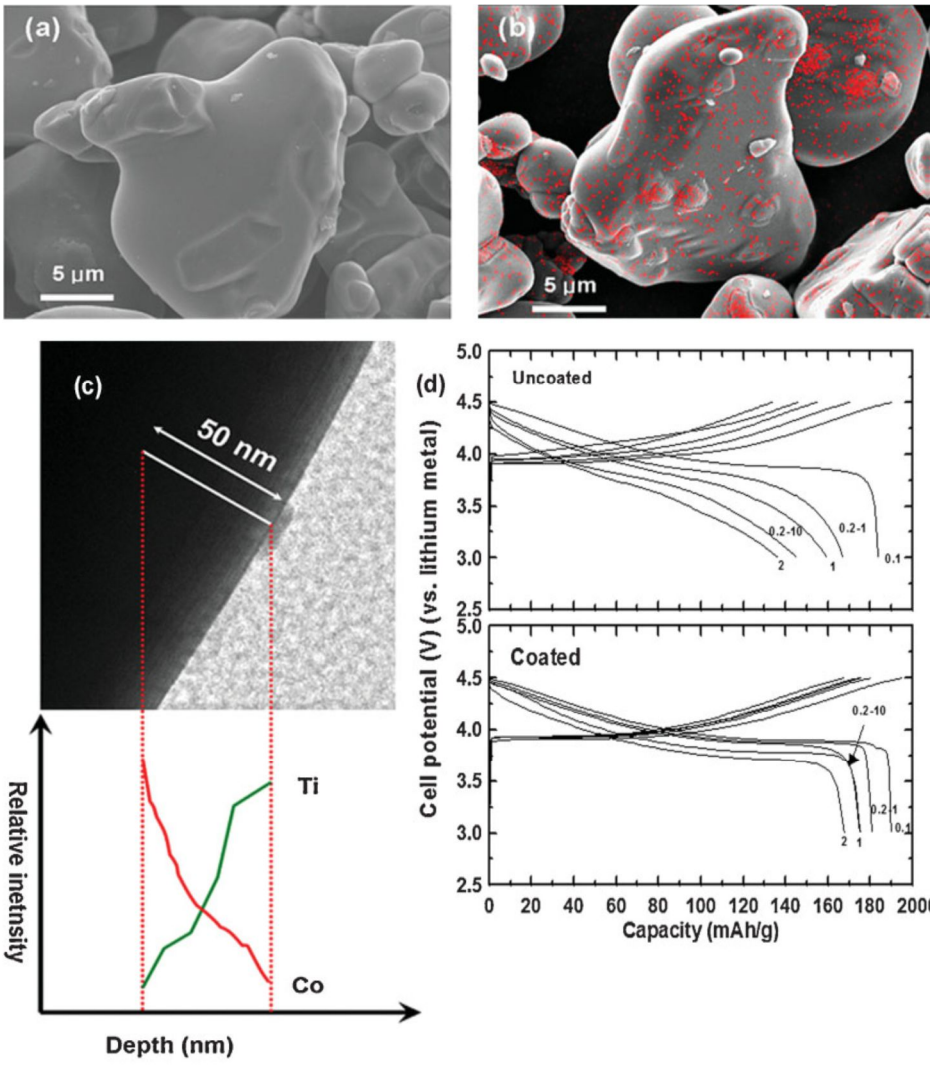


**Figure 4**. a, b) SEM images of the uncoated and $TiO_2$-coated $LiCoO_2$ bulk particle (20mm; red dots are mapping of Ti element). c) Line mapping of Co and Ti elements along the line from surface to the inner part of the coated $LiCoO_2$ particles. d) Voltage profiles of the uncoated and coated $LiCoO_2$ cathodes at different C rates (0.2-1 and 0.2–10 denote first and tenth cycles at a rate of 0.2 C).

# III. EXPERIMENT

In order to prepare $SiP_2O_7$, 5g of $SiO_2$ (particle size was <50nm) and 7.5g of $H_3PO_4$ were mixed in 50ml of distilled water and stirred at 400rpm for 3h and dried at 100°C for 24h. The dried $SiP_2O_7$ powders were ball-milled at 400 rpm for 3h to get an average particle size of ~ 100nm. 100 nm-sized $SiP_2O_7$ nanoparticles were physically mixed with 10 μm-sized $Ni_{0.5}Co_{0.2}Mn_{0.3}(OH)_2$ precursors in a mechanical mixer with a rotating speed of 150 rpm for 20 h. Amount of $SiP_2O_7$ used was 1wt% of the precursors. The detailed coprecipitation method of $Ni_{0.5}Co_{0.2}Mn_{0.3}(OH)_2$ is described in Ref. 3. The dried $SiP_2O_7$-coated $Ni_{0.5}Co_{0.2}Mn_{0.3}(OH)_2$ powders was mixed with $LiOH{\cdot}H_2O$ and were fired at 800°C for 16h in air at a molar ratio of 1:1.02.

A coin-type half cell (2016-size) contained a test electrode, a lithium-metal counter-and-reference electrode, a 15 μm-thick micro-porous polyethylene separator, and an electrolyte solution of 1.01 M $LiPF_6$ in ethylene carbonate (EC)/dimethyl carbonate (DMC) (1:1 vol. %) (LG Chem., Korea). Normally the amount of active materials in the cathode composite was 20 mg. The cathodes for the battery test cells were made from the cathode material, Super P carbon black, and polyvinylidene fluoride (PVdF) binder (Solef) in a weight ratio of 90:5:5. The electrodes were prepared by coating a cathode-slurry onto an Al foil followed by drying at 130°C for 20 min, finally followed by a roll-pressing. For cycling tests, 3 identical cells were used, and the standard deviation of the cells was ± 3 mAh/g.

Powder X-ray diffraction (XRD) (D/Max2000, Rigagu) measurements using Cu Kα radiation were used to identify the phases. The surface of the uncoated and coated samples were observed using scanning electron microscopy (SEM) (JSM 6400, JEOL) and transmission electron microscopy (TEM) (JEOL 2010F). TEM samples were prepared by the evaporation of the dispersed particles in acetone or hexane on carbon-coated copper grids.

X-ray photoelectron spectroscopy (XPS) analyses were performed with a Thermo Scientific K-Alpha spectrometer using a monochromatic Al Kα radiation of energy beam (1486.6eV). Spectra were recorded in the constant pass energy mode at 50.0eV, using a 30μm diameter analysis area. For depth profile, etch time for 0 to 285 sec was used. Before etching, the surface of the electrode was covered with the composite of binder and carbon black, $Ni^{2+}$ and $Ni^{3+}$ peaks could not be obtained. However, etching into > 5nm depth led to observe well resolved $Ni^{2+}$ and $Ni^{3+}$ peaks. Change of the oxidation states of the Si in $SiO_2$ was estimated from peak position, and reference $SiO_2$ thin film was used to estimate the etched depth.

Nano Secondary Ion Mass Spectrometry (Nano-SIMS) analyses were carried out in the CAMECA Nano SIMS 50 instrument. The data in this study were obtained in multi-collection mode by sputtering the sample with a Cs+ primary ion beam, focused into a ~50nm diameter spot and

rastered across an area of 15 μm x 15 μm. The samples were polished until the mid-sections of the cathode material. A pre-sputtering of the surface was performed before measurement in order to eliminate the surface contamination. Images were obtained by collecting simultaneously the four different ions of $^{7}Li^{16}O^{-}$, $^{28}Si^{-}$, $^{31}P^{-}$.

Electrochemical impedance spectroscopy (EIS) data were collected before and after 40 cycles at 60°C with ac amplitude of 10 mV in the frequency range of 0.5 MHz to 10 mHz by an Ivium impedance analyzer. EIS measurements of the cell before and after cycling were done after cell assemblage and after discharging to 3V, respectively. All the fittings were carried out with Solatron software "Zview" with "fit circle" function after discharged to 3V.

Differential scanning calorimetry (DSC) samples of the cathodes were prepared by charging the coin cells to 4.5 V at a 0.1 C rate, followed by holding them at that potential for 2 h. The soaked electrodes with the electrolytes was extracted in the dry-room (moisture content was below 100 ppm) and transferred to aluminum pan. The aluminum pan was sealed with no additional electrolyte or solvent added. X-ray diffraction patterns of the samples were recorded in situ upon increasing temperature by using a high temperature furnace on High Power X-Ray Diffractometer (Rigaku, D/MAZX 2500V/PC) with Cu Kα radiation. The cells were charged to 4.5V and then dissemble electrodes were prepared in the dry-room. The dissembled electrodes were washed with dimethyl carbonate (DMC) solvent for several times and dried in the dry-room and then attached to the sample holder of the furnace. Each pattern was recorded at every 25°C from 150 to 325°C with a step of 4 °$min^{-1}$ in the 15 – 70 °(2θ) range. The temperature was maintained while the patterns were recorded. The electrode was heat at a rate of 5°C $min^{-1}$.

# IV. RESULTS AND DISCUSSIONS

**Figure 5a** shows schematic views of the preparation procedure for the $SiP_2O_7$ coating of the cathode. $Ni_{0.5}Co_{0.2}Mn_{0.3}(OH)_2$ precursor was first mixed with $SiP_2O_7$ nanoparticles prepared from $SiO_2$ nanoparticles and $H_3PO_4$ in an alcohol solution using a mixer at 200 rpm. It was then dried at 120°C. Finally, a stoichiometric mixture of $LiOH{\cdot}H_2O$ and $SiP_2O_7$-coated $Ni_{0.5}Co_{0.2}Mn_{0.3}O_2$ particles was fired at 800°C for 16h. **Figure 5b** shows SEM images of $Ni_{0.5}Co_{0.2}Mn_{0.3}(OH)_2$ and annealed $LiNi_{0.5}Co_{0.2}Mn_{0.3}O_2$ particles after $SiP_2O_7$ coating. After annealing at 800°C, the cathode shows increased primary particles size, compared to $Ni_{0.5}Co_{0.2}Mn_{0.3}(OH)_2$.

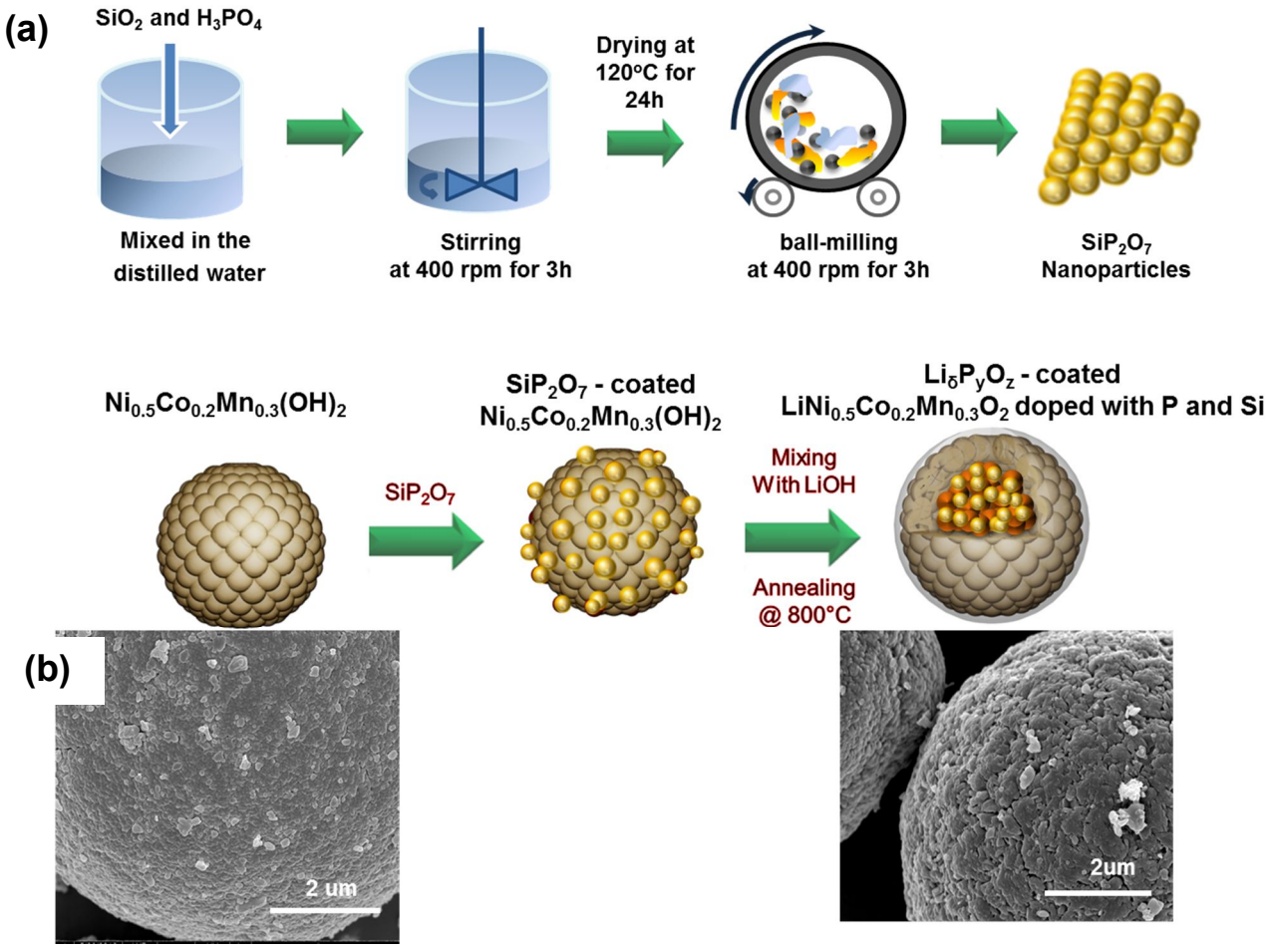


**Figure 5**. **(a)** Schematic views of the preparation procedure for the $SiP_2O_7$ coating on the cathode and (b) SEM images of $Ni_{0.5}Co_{0.2}Mn_{0.3}(OH)_2$ and annealed $Ni_{0.5}Co_{0.2}Mn_{0.3}O_2$ particles after $SiP_2O_7$ coating at 800°C for 16h.

Phase and stoichiometry of ball-milled $SiP_2O_7$ was confirmed by inductively coupled plasma-atomic emission spectroscopy (ICP-AES) and XRD pattern (**Figure 6a**). SEM image of the ball-milled $SiP_2O_7$ shows the particle size of ~ 100 nm (**Figure 6b**). Since we used stainless steel balls, possible reaction with $SiP_2O_7$ is believed to be rarely occurred.

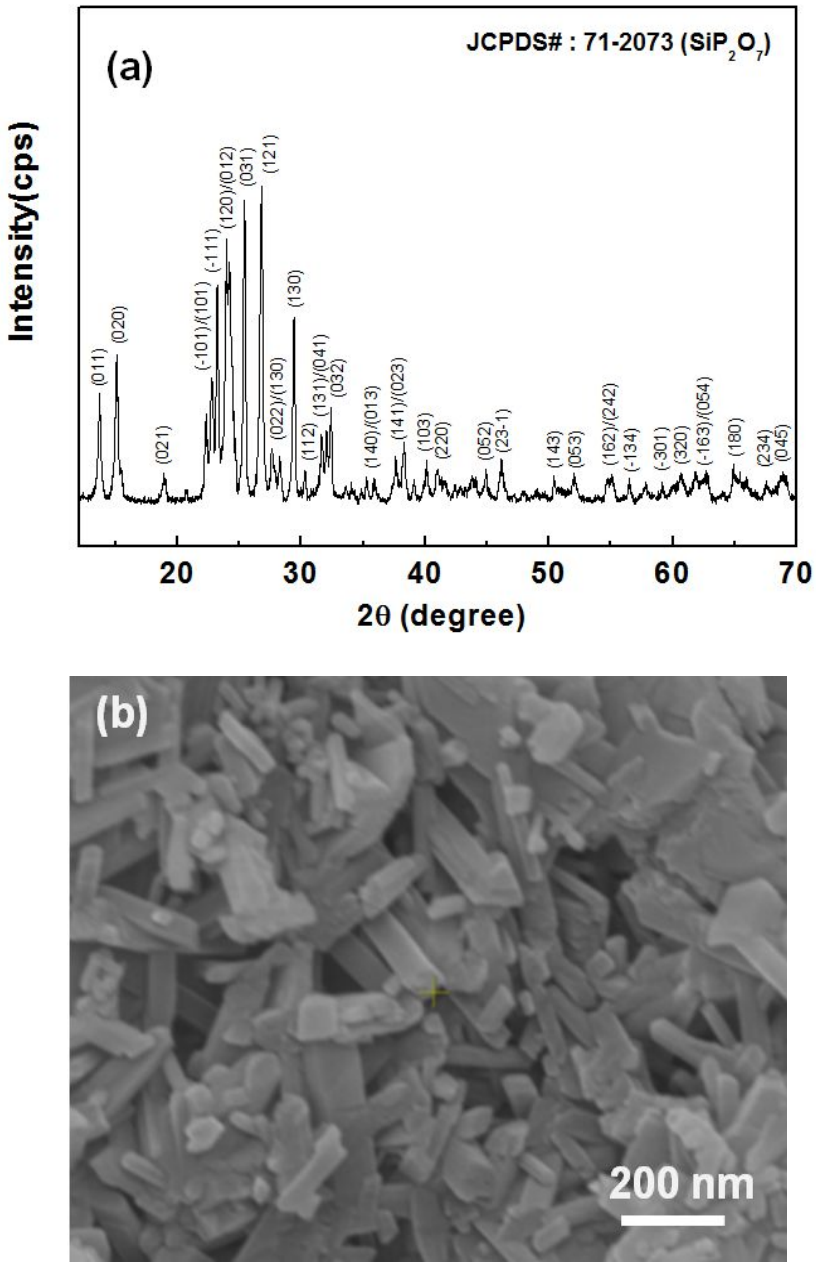


**Figure 6**. (a) Power XRD pattern and (b) SEM image of as-prepared $SiP_2O_7$ nanoparticles.

**Figures 7 a and b** shows the powder XRD patterns and fitted profiles of a $LiNi_{0.5}Co_{0.2}Mn_{0.3}O_2$ cathode before and after $SiP_2O_7$ coating (1 wt%) using Rietveld method, indicating the formation of a layered R-3m phase. The $SiO_2$-coated $LiNi_{0.8}Co_{0.2}O_2$ cathode obtained from the decomposition of $SiH_4$ at 300°C demonstrated the presence of both $Si^{4+}$ and $Si^{2+}$ ions based upon XPS analysis [2]. Similarly, $SiO_2$-coated $LiNi_{0.8}Co_{0.15}Al_{0.05}O_2$ cathode reported possible formation of $Si^{2+}$ in the cathode based upon XPS analysis [24].

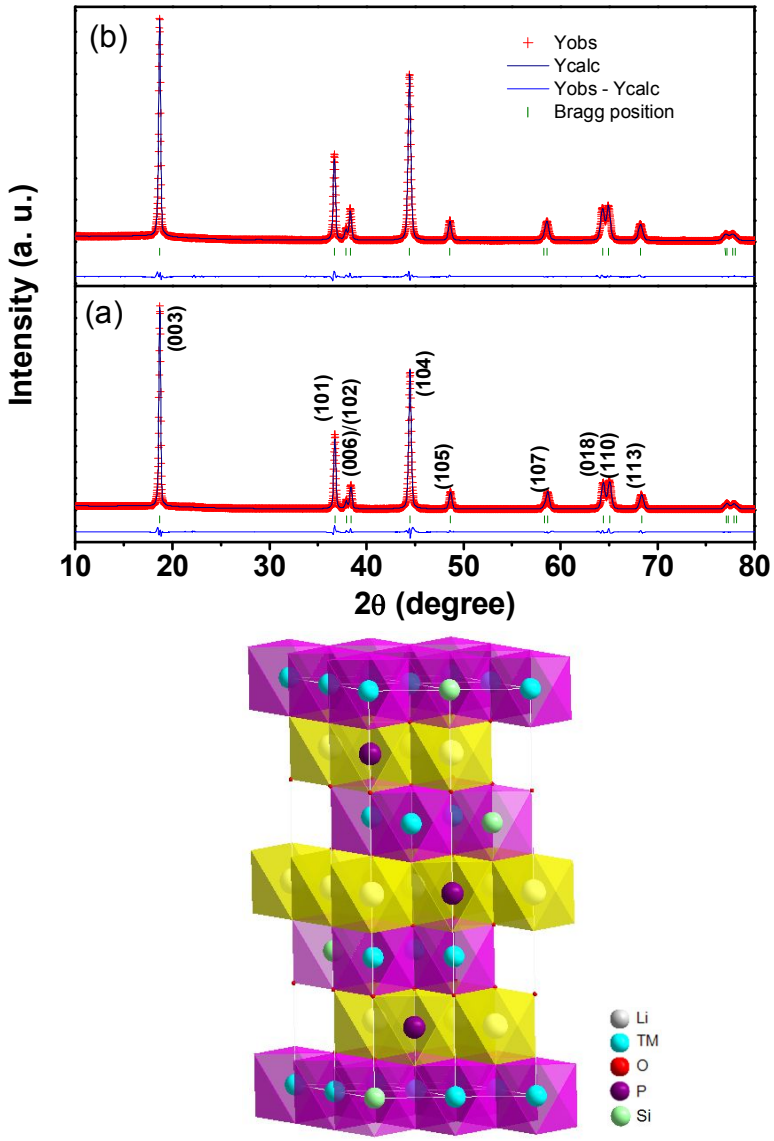


**Figure 7**. Powder XRD profiles and the fitted profiles of (a) the pristine $LiNi_{0.5}Co_{0.2}Mn_{0.3}O_2$ (b) coated $LiNi_{0.5}Co_{0.2}Mn_{0.3}O_2$, respectively. Reliability factors (R-factor) obtained from the fitting are as follows: the pristine $LiNi_{0.5}Co_{0.2}Mn_{0.3}O_2$ : $R_p$ = 4.69, $R_{wp}$ = 6.70, $R_{exp}$ = 3.88; coated $LiNi_{0.5}Co_{0.2}Mn_{0.3}O_2$ : $R_p$ = 3.38, $R_{wp}$ = 4.95, $R_{exp}$ = 3.84, and (c) proposed structure of the coated cathode based upon the fitting.

**Table 1** shows refined lattice constants and fractional occupation number of *3a* sites in Si, P elements and shows the possible presence of Si ions in the 3*a* sites. The lattice constants *a* and *c* of the pristine sample were 2.8647(4) and 14.225(2)Å, respectively. However, after the coating procedure their values slightly decrease to 2.8637(3) and 14.219(5)Å, respectively [90]. The ionic radii of $Si^{4+}$ and $Si^{+}$ are 0.4 and 0.65 Å, respectively, and therefore $Si^{4+}$ and $Si^{2+}$ ions can be substituted into *3a* Li sites and *3b* transition metal sites, respectively. Similar to this, $P^{5+}$ (0.38 Å) ions are also taken into 3*a* sites (**Fig. 7C**). Based upon Rietveld method, most of Si and P ions placed in 3*a* sites. This is why occupancy ratio of 3b sites remains almost similar to that before coating. Therefore, this result along with such a decrease in the lattice constants also indicates the formation of $LiNiCo_{0.2}Mn_{0.3}O_2$ solid solution phase doped with Si and P ions as a result of the reaction between $Si_2P_2O_7$ and $LiNi_{0.5}Co_{0.2}Mn_{0.3}O_2$ at 800°C. A contraction of the lattice parameters has been reported to induce structural stability. For instance, Co and Al substitutions for Ni in $LiNiO_2$ result in shrinkage of the *a*-axis as the radii of $Co^{3+}$ and $Al^{3+}$ are smaller than that of $Ni^{3+}$, which is considered to be origin of the stabilization of the layered structure of the $LiNi_{0.8}Co_{0.15}Al_{0.05}O_2$ cathode [91].

**Table 1.** Rietveld refinement result of pristine $LiNi_{0.5}Co_{0.2}Mn_{0.3}O_2$ and coated $LiNi_{0.5}Co_{0.2}Mn_{0.3}O_2$ samples

| Sample | pristine | | coated | |
|---|---|---|---|---|
| Lattice constants | *a* (Å) | *c* (Å) | *a* (Å) | *c* (Å) |
| | 2.8647(4) | 14.225(2) | 2.8637(3) | 14.219 (5) |
| Fractional occupancies | | | | |
| Li on *3a* sites | 0.99 | | 0.97 | |
| Si and P on *3a* sites | | | 0.03 | |
| Transition metals on 3*b* sites | 0.99 | | 0.99 | |
| Si on 3*b* sites | | | 0.01 | |

**Figure 8** shows the nano-SIMS (secondary ion mass spectroscopy) spectra of Si and P and Li in a cross-sectioned coated sample. This is the first report of a distribution of high-resolution element mapping including Li in the particle with a lateral resolution of < 50 nm. In the case of Li, it is distributed uniformly throughout the sample, though the distribution was impossible to obtain using EPMA (electron probe micro-analysis).

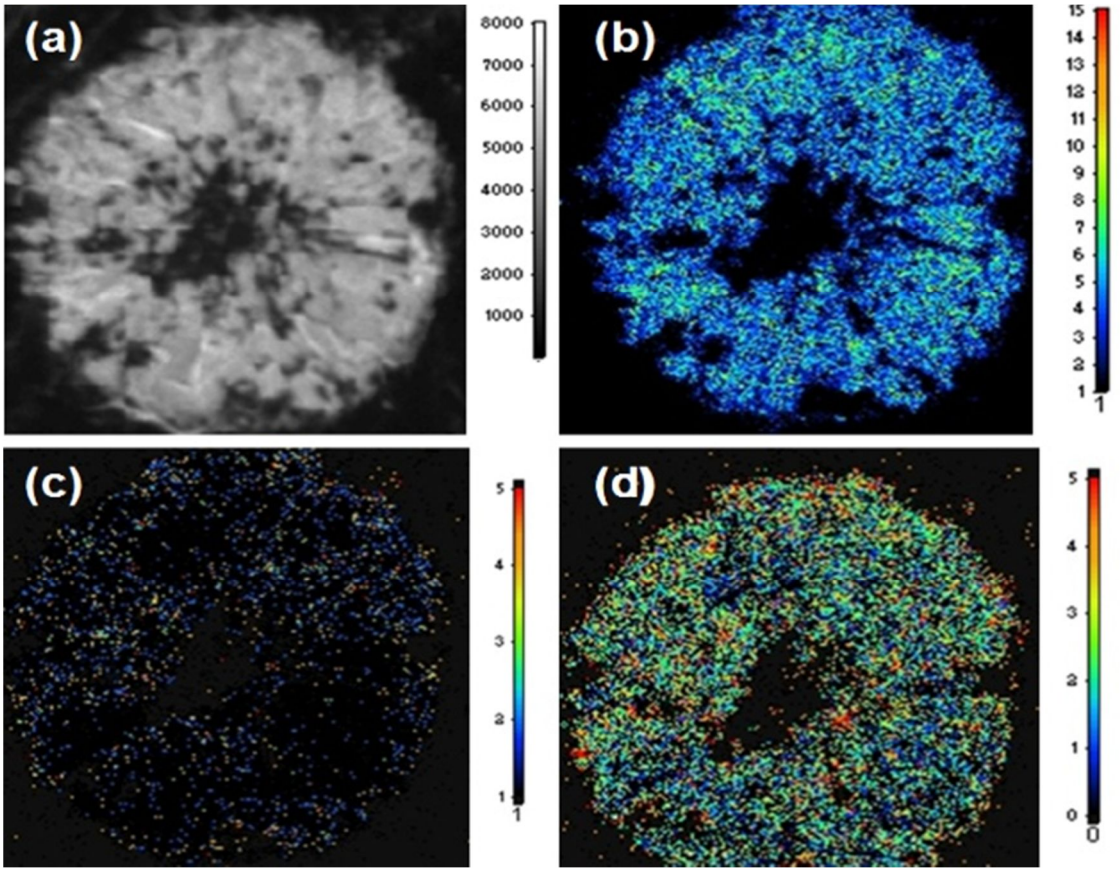


**Figure 8**. Nano-SIMS of cross-sectioned coated $LiNi_{0.5}Co_{0.2}Mn_{0.3}O_2$ cathode particle (a: cross-sectioned image, b: mapping of lithium, c: mapping of P, and d: mapping of Si)

Quite similar to this behavior, S and P elements are distributed rather uniformly, supporting the solid solution phase. The XPS spectra of Ni ($2p_{3/2}$), Co($2p_{3/2}$), and Mn($2p_{3/2}$) in the $LiNi_{0.5}Co_{0.2}Mn_{0.3}O_2$ cathode confirm that the oxidation state of Ni is a mixture of $Ni^{2+}$ and $Ni^{3+}$ and $Co^{3+}$ and $Mn^{4+}$ (**Figure 9**), which agrees with an earlier result [21].

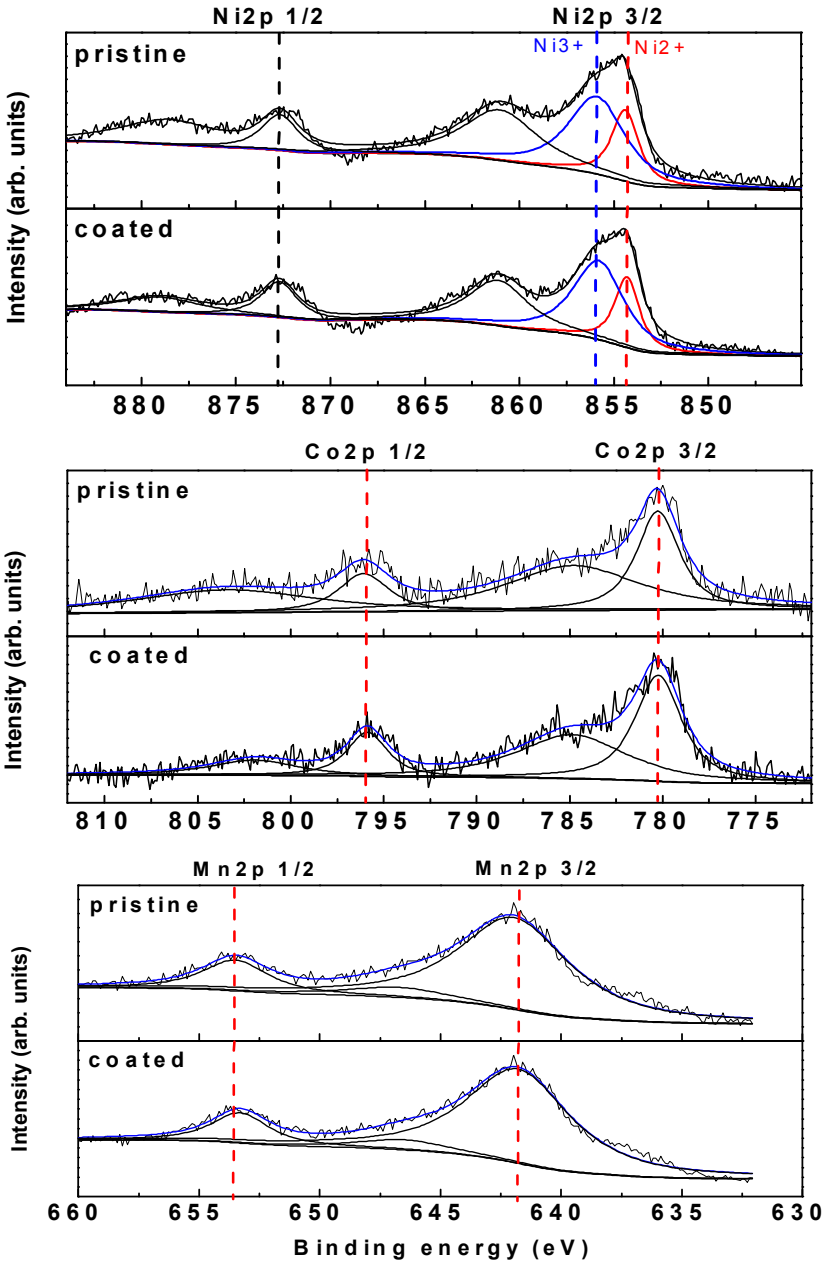


**Figure 9**. XPS of (a) Ni2p, (b) Co2p, and (c) Mn2p in the pristine and coated $LiNi_{0.5}Co_{0.2}Mn_{0.3}O_2$.

**Figure 10** shows XPS analyses of Si and P in a coated sample after etching for 10 nm (after removing the binder layer) and $SiP_2O_7$ nanoparticles. Here, peaks assigned to $Si_2P_2O_7$ cannot be observed in the coated sample. Instead, peaks assigned to SiO and $SiO_2$ are present. This result indicates that the oxidation states of Si in the solid solution phase are either 2+ or 4+. The $P2p_{3/2}$ spectrum of the coated sample shows a broad peak centered at 135 eV, which agrees with the $Li_4P_2O_7$ result, but the possible formation of a $Li_3PO_4$ phase with a peak centered at 133.8 eV cannot be excluded.

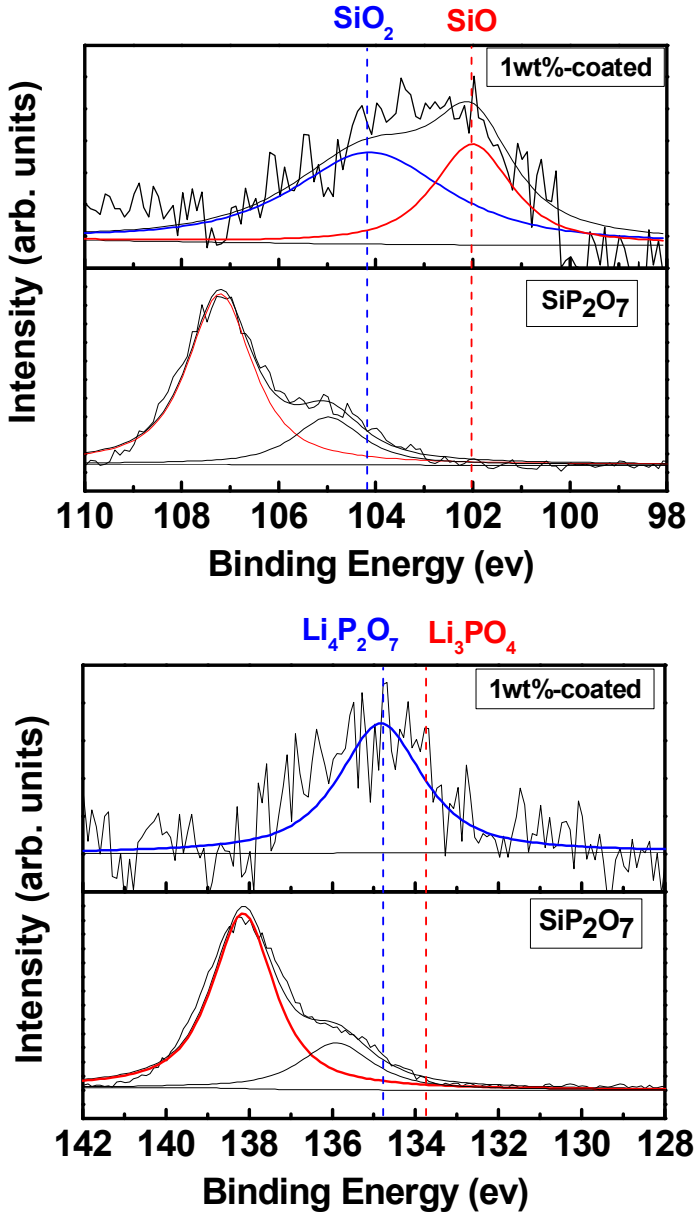


**Figure 10**. XPS of (a) $Si2p_{3/2}$ and (b) $P2p_{3/2}$ in the coated $LiNi_{0.5}Co_{0.2}Mn_{0.3}O_2$ and $SiP_2O_7$ nanoparticles.

This indicates that the $SiP_2O_7$ layer reacted with LiOH completely and that some parts of $Li_\delta P_yO_z$ remained on the surface while the remaining parts were formed in the solid solution. TEM image of the coated samples show the amorphous coating layer with a thickness of < 2 nm (**Fig. 11a**), and we believe that this layer is consisted of $Li_\delta P_yO_z$. Also, note that digitalized Fourier-transformed image of the expanded image of **Fig. 11a** confirms that coating layer is clearly identified as amorphous phase (**Fig. 11b**). Inner parts of the coating layer consist of layered phase, confirmed by (-102), (0-1-2), and (2-21) planes from digitalized Fourier-transformed images. In consequence, after the $SiP_2O_7$ coating, a $LiNi_{0.5}Co_{0.2}Mn_{0.3}O_2$ solid solution doped with Si and P ions was formed with an amorphous $Li_\delta P_yO_z$–like coating layer.

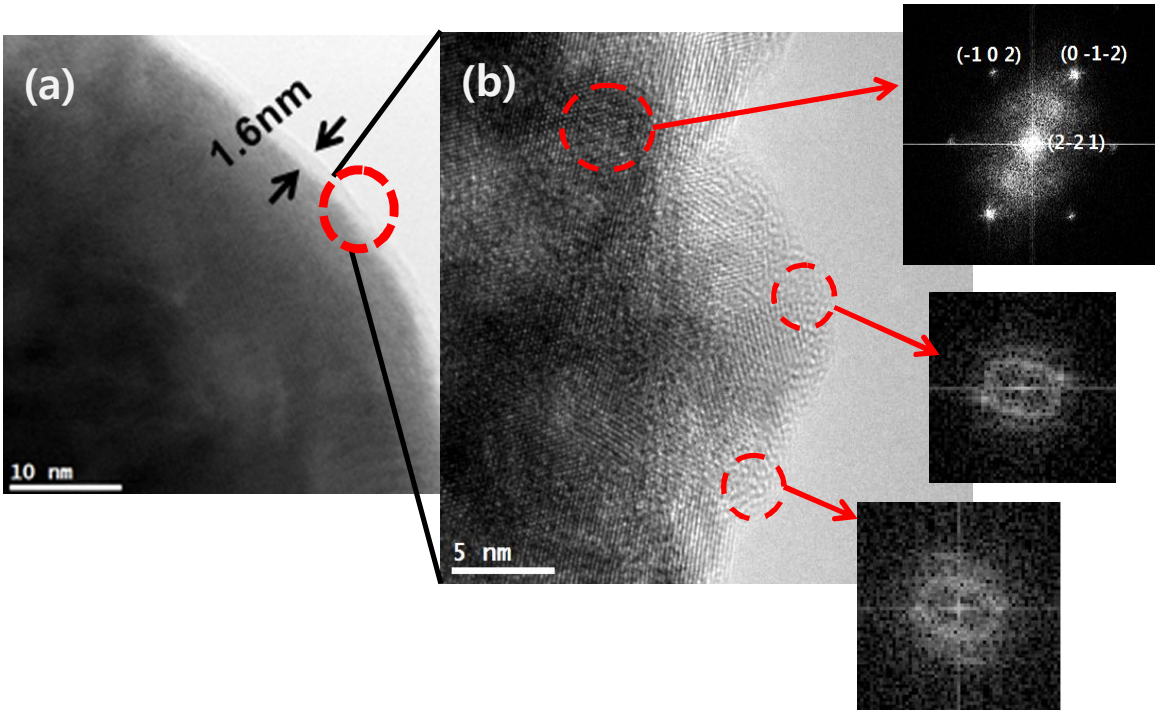


**Figure 11**. (a and b) TEM images of the coated $LiNi_{0.5}Co_{0.2}Mn_{0.3}O_2$. (b) is high resolution TEM image of dotted area of (a) and digitalized Fourier-transformed images of red dotted areas of (b).

To observe the electrochemical performance of the cathodes, a rate capability assessment up to a rate of 7C under same charge and discharge rates a 21$^{o}$C were carried out, as shown in **Figure 12a**. Pristine and coated samples were cycled between 4.5 and 3V while increasing the C rate from 0.2 to 7C in lithium half cells (2016R type) (1C corresponds to 185 $mAg^{-1}$ and the amount of active material in the composite electrode was 20 mg and charge and discharge rates were same). The discharge capacities of the pristine sample were found to be 185, 161, 112 and 45 mAh/g at rates of 0.2, 1, 3 and 5C, but its capacity dropped to zero at a rate of 7C (= 1.26 A/g). However, the coated sample exhibited substantially enhanced values of 174, 153, 125 and 104 $mAhg^{-1}$, respectively, and a further increase in the C rate to 7C resulted in 83 $mAhg^{-1}$. The decreased capacity of the coated sample at a 0.2C rate is due to decreased amounts of electroactive $Ni^{2+}$ or $Ni^{3+}$ ions as a result of increased Si and P ions in 3b sites. **Fig. 12b** shows the discharge capacity of the pristine and coated cathodes as a function of the cycle number under increasing C rates. In contrast to the pristine sample that shows a slow capacity fade at 5C rate, the coated samples show no capacity fades during cycling both at 5 and 7C rates. In order to make sure of reproducibility, three coin-cells containing same pristine samples were tested.

In terms of the rate capability, it was reported that an amorphous $Li_4P_2O_7$-like coating layer on the $LiFePO_4$ cathode resulted in in significantly improved rate capability at higher rates [92]. R ecent molecular dynamic research findings proposed that the major enhancement of the LiFeP $O_4$ was due to the overall $Li^+$ ion mobility increase of nearly two orders of magnitude in the vicinity of the interface between the ionic conducting $Li_4O_2P_7$-like layer and the $LiFePO_4$ [93] . This enhancement was proposed to be related to the fast electrostatic energy storage by $Li^+$ in the interface region ($Li_4P_2O_7/LiFePO_4$) and the significant potential for enhanced $Li^+$ ion conductivity by the mesoscopic multiphase effect [93, 94]. In addition, the domino-cascade model of $LiFePO_4$ suggests that the strategy for manipulating $LiFePO_4$ nanoparticles should entail surface modification to decrease the charge transfer resistance between the electrode and electrolyte [95, 96]. In these regards, it can be concluded that remarkablely improved rate capability of the coated cathode is due to the amorphous coating layer and is not related to the bulk phase.

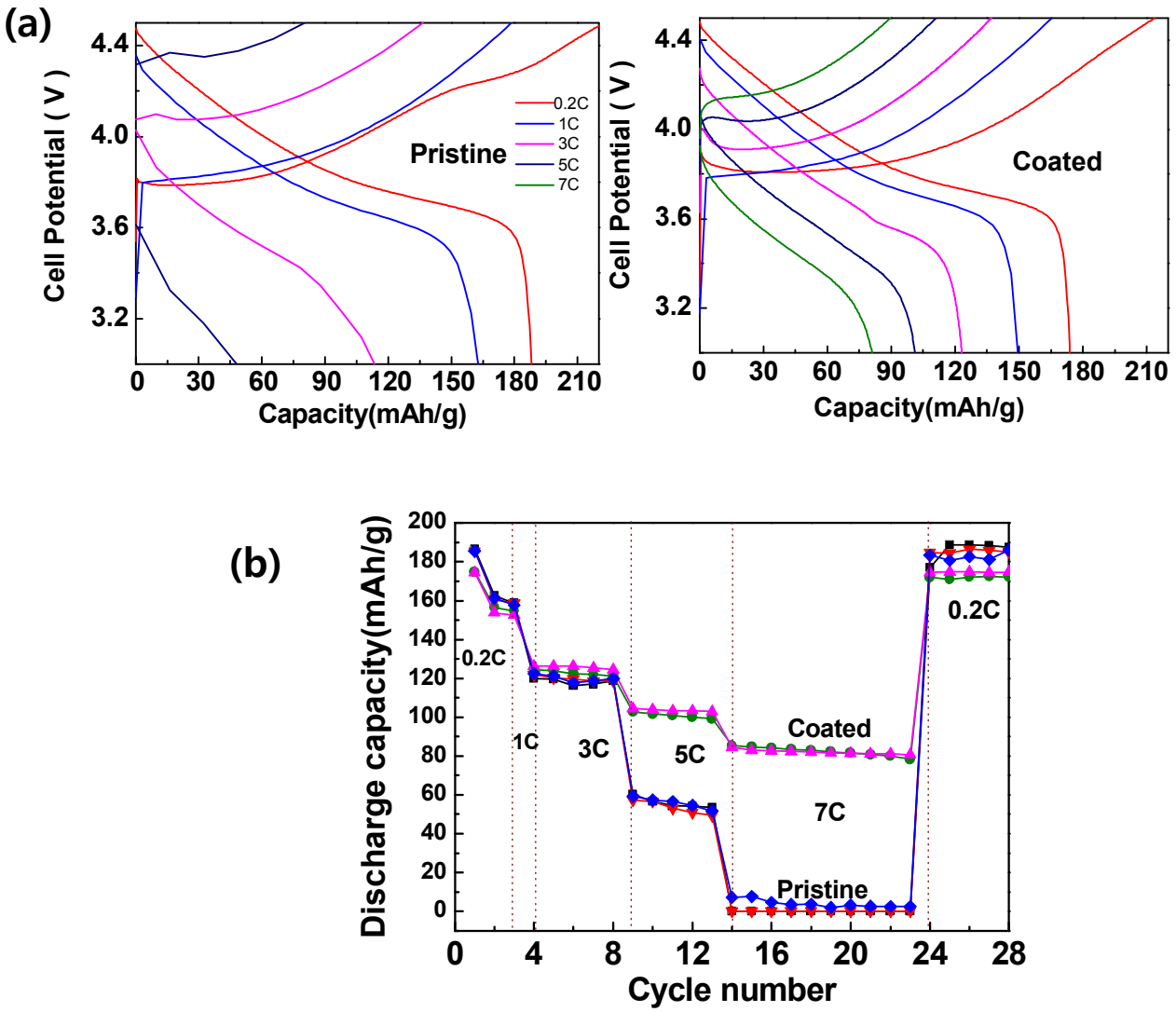


**Figure 12. (a)** Voltage profiles of pristine and coated $LiNi_{0.5}Co_{0.2}Mn_{0.3}O_2$ cathodes between 4.5 and 3V while increasing the C rate from 0.2 to 7C in lithium half cells (2016R type) at 21°C and (b) rate capability test of (a) from 0.2 to 7C rates. 1C was set at 185 $mAg^{-1}$ and charge and discharge rates are same and three identical coin-cells were used for pristine sample test.

In addition, we estimate the changes of the working voltages (the working voltage corresponds to the voltage of half of the value of the capacity) at a different rate (**Figure 13**). While charging and discharging, the working voltages of the coated samples are lower during the charge and higher during the discharge than the pristine sample. For instance, the working voltage of the coated sample was 3.44 V at a 7C rate, which is much higher than that of the pristine sample (2.7V). This result indicates that a nanoscale thin $Li_\delta P_y O_z$ coating layer improved the charge transfer reaction characteristics and lithium ion diffusivity at the interface. This result supports the previous result in which the charge transfer resistance was found to be one of the dominant sources of resistance[95]. High level of polarization at high charge-discharge rates is resulted from slow lithium diffusion or low electric conductivity in the active material, thus leading to rapid initial drop of voltages. This phenomenon is well presented by the voltage profiles at higher rates.

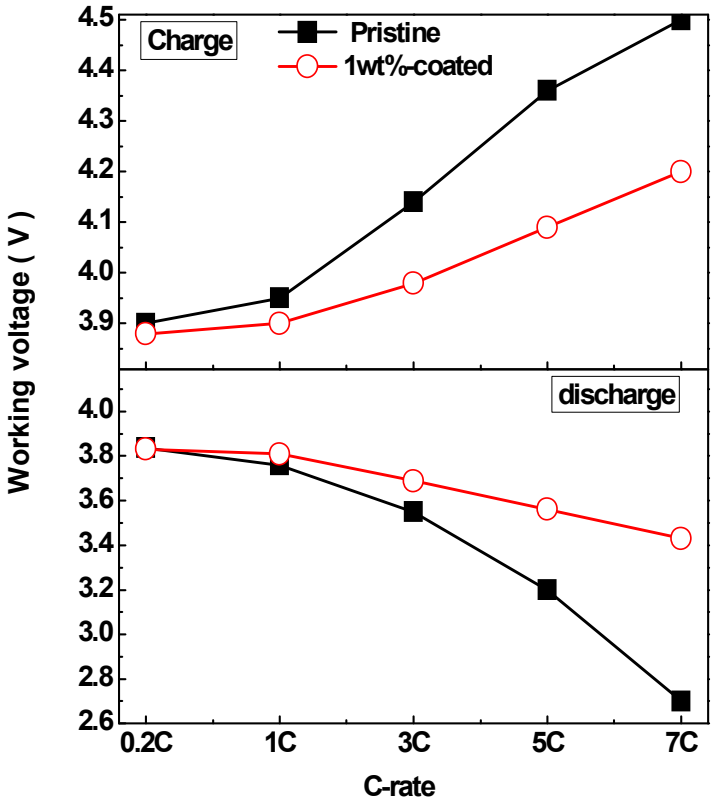


**Figure 13**. Plots of working voltage (cell potential at a half value of the discharge or charge capacities) in the pristine and coated $LiNi_{0.5}Co_{0.2}Mn_{0.3}O_2$ with increasing C rates from 0.2 to 7C at 21°C.

**Figure 14** shows a plot of the discharge capacity as a function of the cycle number for a pristine and a coated cathode in lithium half cells at 60°C. The discharge capacities of prstine and coated samples exhibit reversible capacities of 183 and 182 $mAhg^{-1}$ at a 0.5C rate. However, after 40 cycles, the pristine and coated cathode show reversible capacities of 137 $mAhg^{-1}$ and 165 $mAhg^{-1}$, respectively, corresponding to 74% and 91% retention.

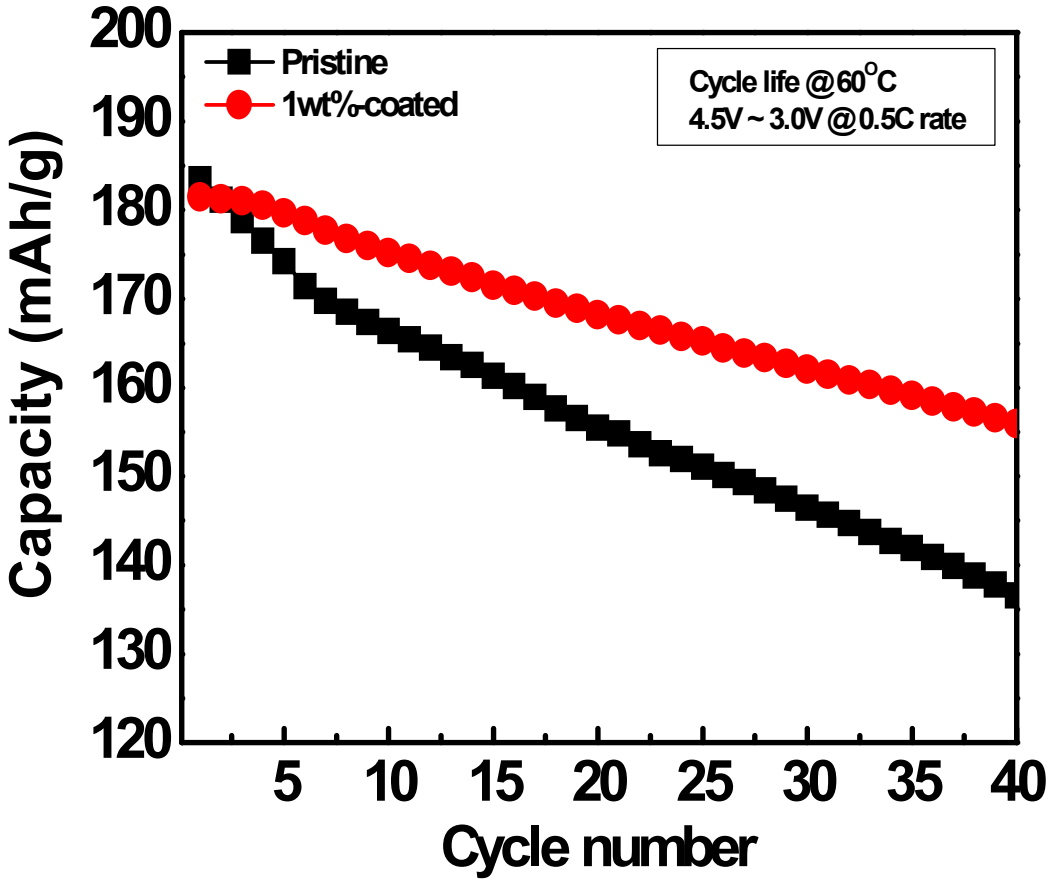


**Figure 14**. Plot of discharge capacuty as a function of cycle number in lithium half cells containing pristine and coated $LiNi_{0.5}Co_{0.2}Mn_{0.3}O_2$ cathodes between 4.5 and 3V at 60°C. Cells were cycled at a rate of 0.5C.

To observe the changes of the electrode materials after cycling at 60°C, electrochemical impedance and XPS analyses were carried out. **Figure 15** shows Nyquist plots of coin-type half cells containing pristine and coated cathodes before and after the tests as well as the interfacial behavior between them. The electrolyte can be investigated using a possible equivalent circuit as proposed in earlier research (**Figure 15**). The values of $R_{SEI}$ (surface film resistance) and $R_{ct}$ (charge transfer resistance) can be estimated from the Nyquist plot. Before cycling, the $R_{ct}$ value of the pristine cathode was smaller than that of the coated sample, which could be related to the presence of a pure ionic conducting $Li_xP_yO_z$-like coating layer. After cycling, the values of $R_{SEI}$ and $R_{ct}$ in the coated sample were found to be much smaller than those in the pristine sample, at almost 1/5 of the value. The increased surface film and charge-transfer resistances are indicative of the formation of a larger fraction of the nonconducting interfacial films as a result of enhanced side reactions with the electrolytes [12, 97, 98].

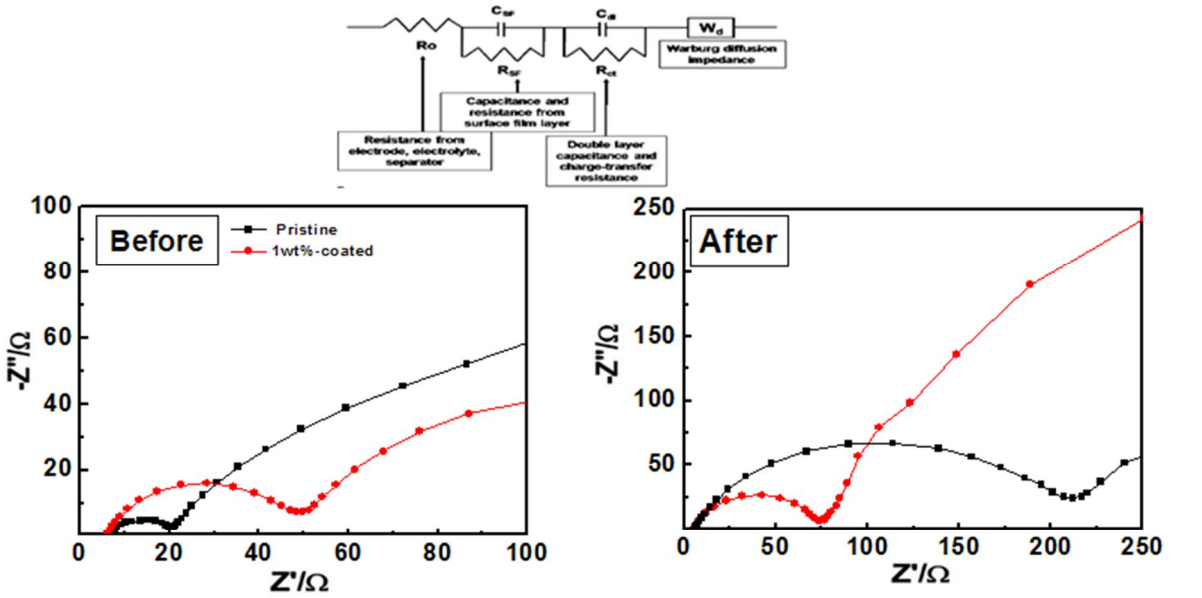


| before | $R_0$ (Ω) | $R_{SEI}$ (Ω) | $R_{ct}$ (Ω) |
|---|---|---|---|
| bare | 6.0 | 10.11 | 4.9 |
| 1wt% -coated | 6.0 | 33.1 | 11.2 |

| after | $R_0$ (Ω) | $R_{SEI}$ (Ω) | $R_{ct}$ (Ω) |
|---|---|---|---|
| bare | 6.12 | 51.2 | 155.68 |
| 1wt% -coated | 6.18 | 33.9 | 34.72 |

**Figure 15**. Nyquist plot Plots of the pristine and coated $LiNi_{0.5}Co_{0.2}Mn_{0.3}O_2$ before and after cycling at 60°C. Tables shows esiniated vlaues of $R_o$, $R_{SEI}$, and $R_{ct}$ using the equivalnet curcuit (top).

According to the XPS spectra of the pristine and coated cathode before and after cycling at 60°C at depths of 15, 30, and 60 nm from the surface, the spectra of the coated cathode were quite similar to

those of the pristine sample before cycling. The spectra of the cathodes between 859 and 852 eV could be deconvoluted into $Ni^{2+}$ and $Ni^{3+}$ peaks and were converted to their relative peak area (**Figure 16**).

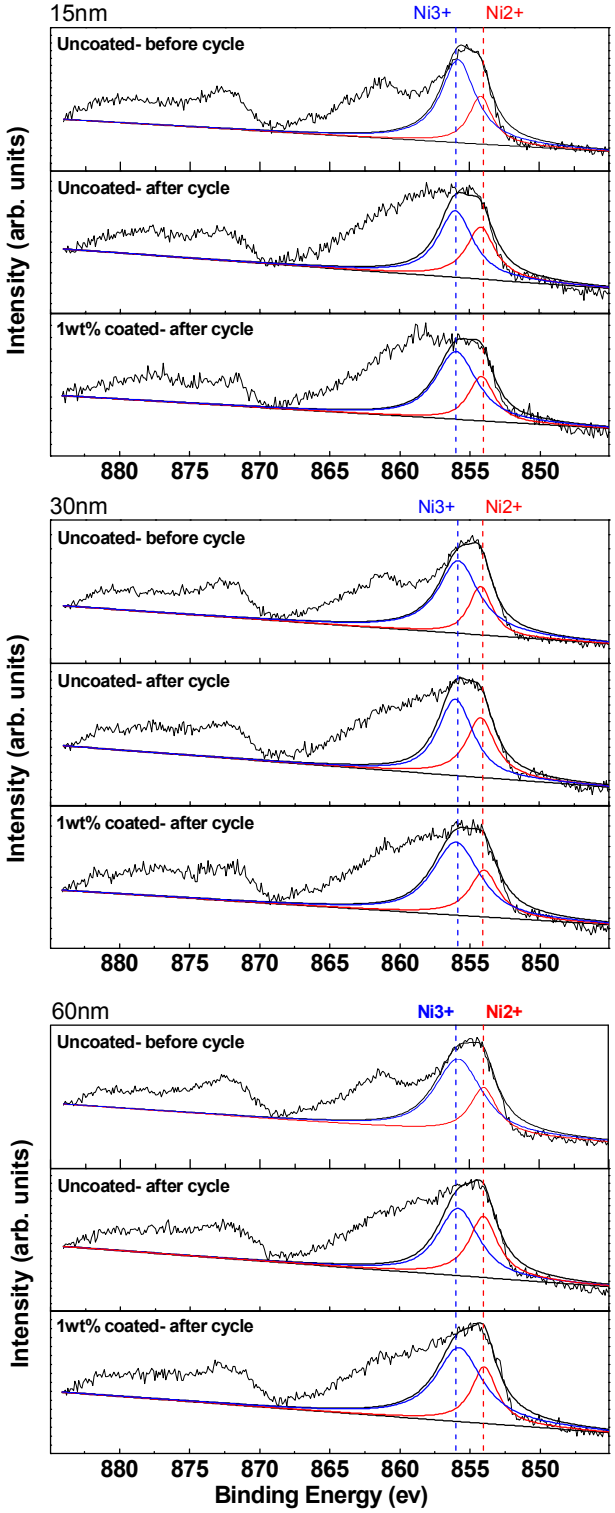


**Figure 16**. XPS of $Ni2p_{3/2}$ of pristine and coated $LiNi_{0.5}Co_{0.2}Mn_{0.3}O_2$ electrodes before and after cycling at 60°C (etching depths were 15, 30, and 60nm).

**Figure 17** shows a plot of the relative amount of $Ni^{2+}$ and $Ni^{3+}$ ions. The coated sample showed no increase in the $Ni^{2+}$ content, while the pristine sample showed a 10% increase. Moreover, the $Ni^{3+}$ content of the pristine sample also showed a decrease. The formation of $Ni^{2+}$ species was likely caused by the spontaneous reduction from $Ni^{3+}$ ions; for instance, NiO formation in conjunction with a loss of oxygen in the lattice is very common in a Ni-rich system[9, 99, 100].

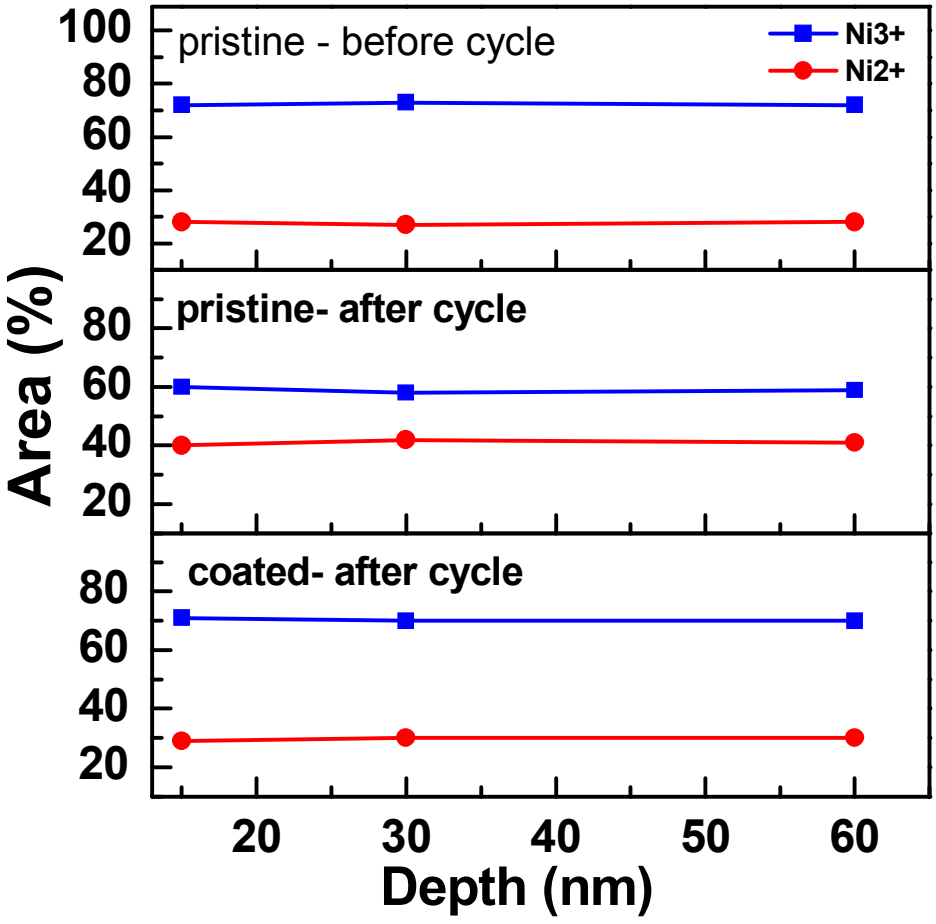


**Figure 17**. Plots of demension ratio of $Ni^{2+}$ and $Ni^{3+}$ peaks of **Figure 16**.

To evaluate the thermal stability of the cathode materials, a DSC (differential scanning calorimetry) analysis was used. Here, the amount of heat generation and the peak height are the critical parameters to measure [101, 102]. To conduct this analysis, we used an electrode soaked with electrolyte after charging it to 4.5V, although many previous works used electrodes charged to 4.3V. After removing the soaked electrode from the Al foil, it was sealed in a high-pressure pan. **Figure 18** shows DSC scans of pristine and coated samples after charging at 4.5 V ($Li_{0.1}Ni_{0.5}Co_{0.2}Mn_{0.3}O_2$) between 100°C and 350°C at a scan rate of 5°C/min.

The pristine sample shows two peaks with an onset temperature of 225°C. The peak area was indicative of the total amounts of oxygen that evolved from the cathode, and this was estimated at 580 J/g. However, the coated sample showed a single peak with a greatly depressed peak height at an onset temperature of 248°C. In addition, the peak area was significantly decreased to 120 J/g. This result clearly indicates that the coating layer and a solid solution $LiNi_{0.5}Co_{0.2}Mn_{0.3}O_2$ phase doped with P and Si ions sustainably reduced the initial exothermic reactions with the electrolytes and improved the structural stability.

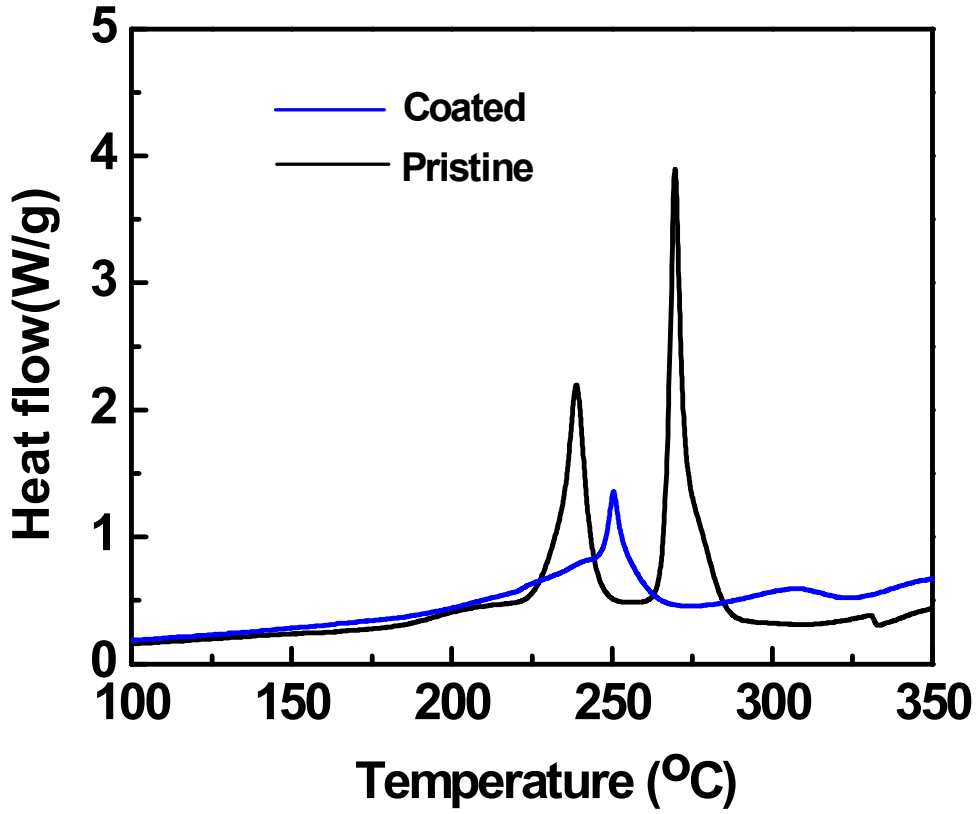


**Figure 18.** DSC scans of pristine and coated $Li_{0.1}Ni_{0.5}Co_{0.2}Mn_{0.3}O_2$ samples after charging at 4.5 V between 100°C and 350°C at a scan rate of 5°C/min.

Such structural stability is supported by the in situ XRD measurements of the samples up to 325°C (**Figure 15).** XRD patterns of pristine sample show two merged diffraction peaks ((108) and (110)) at 200°C, indicating that the layered phase ($Li_{1-z}$ $NiO_2$ (*R-3m*)) decomposed to a cubic spinel phase $Li_zNi_2O_4$ ( *Fd-3m*) [103]. However, the coated cathode materials show the merged peak at 250°C.

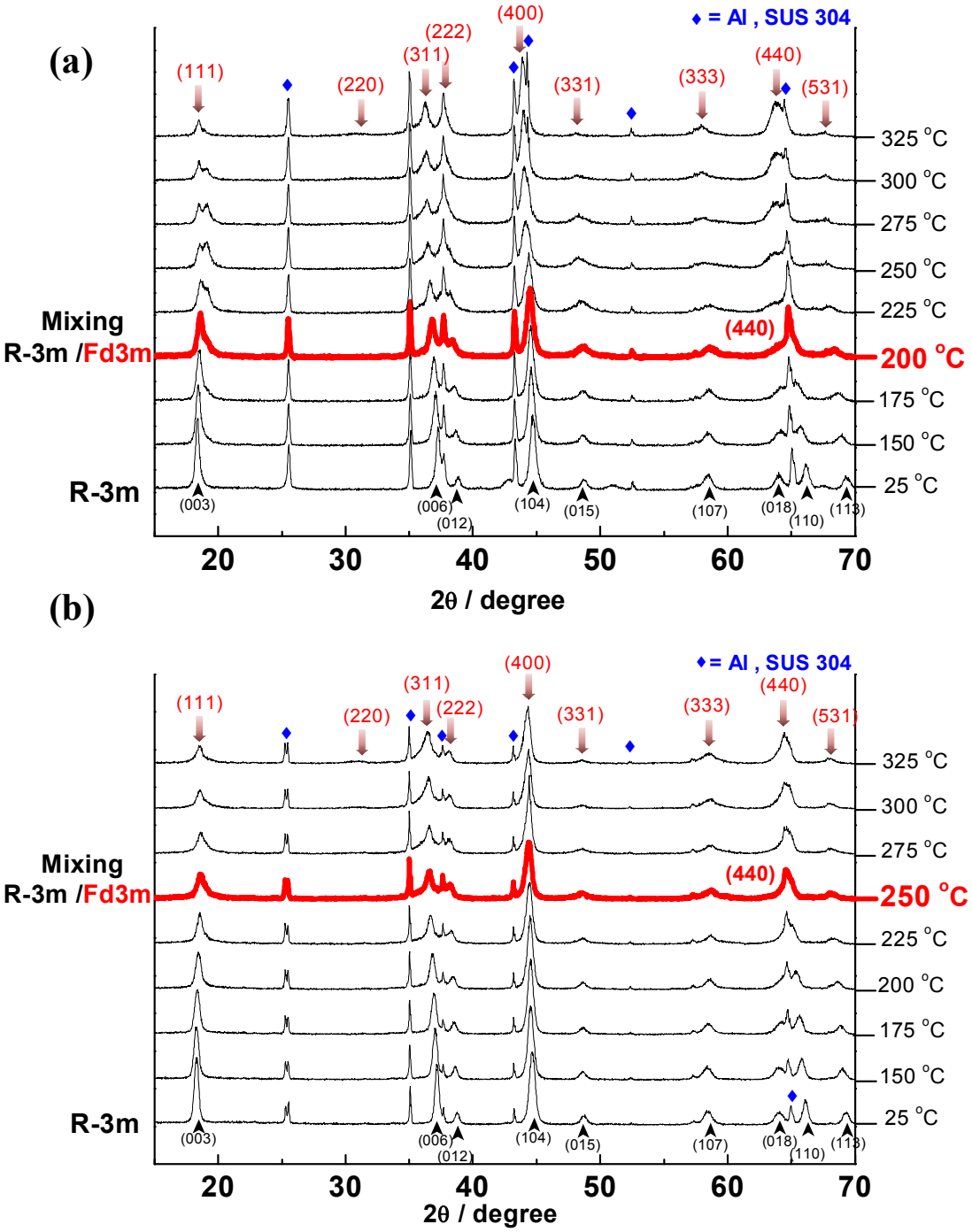


**Figure 19**. In situ XRD patterns of (a) pristine and (b) coated $Li_{0.1}Ni_{0.5}Co_{0.2}Mn_{0.3}O_2$ electrode between 25°C and 325°C under sealed Ar chamber.

Based on the two identified phases (layered and spinel) from the XRD patterns, the values of $a_{hex}$ and $c_{hex}$ constants were reduced to see the evolution of the $c_{hex}/ a_{hex}$ ratio as a function of temperature as proposed by Delmas et al. [103] in **Figure 20**. When the ratio is 4.90, which is the theoretical value for a cubic structure. Both pristine and coated cathode do not completely transformed to the spinel phase even at 250°C, but higher $c_{hex}/ a_{hex}$ ratios of the coated cathodes than the pristine ones both at 200 and 250°C indicates preferred formation of the layered phases. Also, note that thermal transition from the layered to spinel occurs at higher temperatures for the coated cathodes. Accordingly, the coated cathode demonstrated greatly improved structural stability compared to the pristine sample, which is consistent with the DSC result. Previously reported $SiO_2$ or metal phosphate coatings on the cathode mainly focused on the improvement of the cycle life at higher charge cut-off and at 60°C [9, 11, 13]. For instance, $SiO_2$ coating on $LiNi_{0.8}Co_{0.15}Al_{0.05}O_2$ demonstrated enhanced cycling stability at 60°C[12]. In this study, this new cathode material exhibited not only significantly improved rate capability but also suppressed oxygen evolution the lattice at 4.5V above 200°C, compared to the pristine sample.

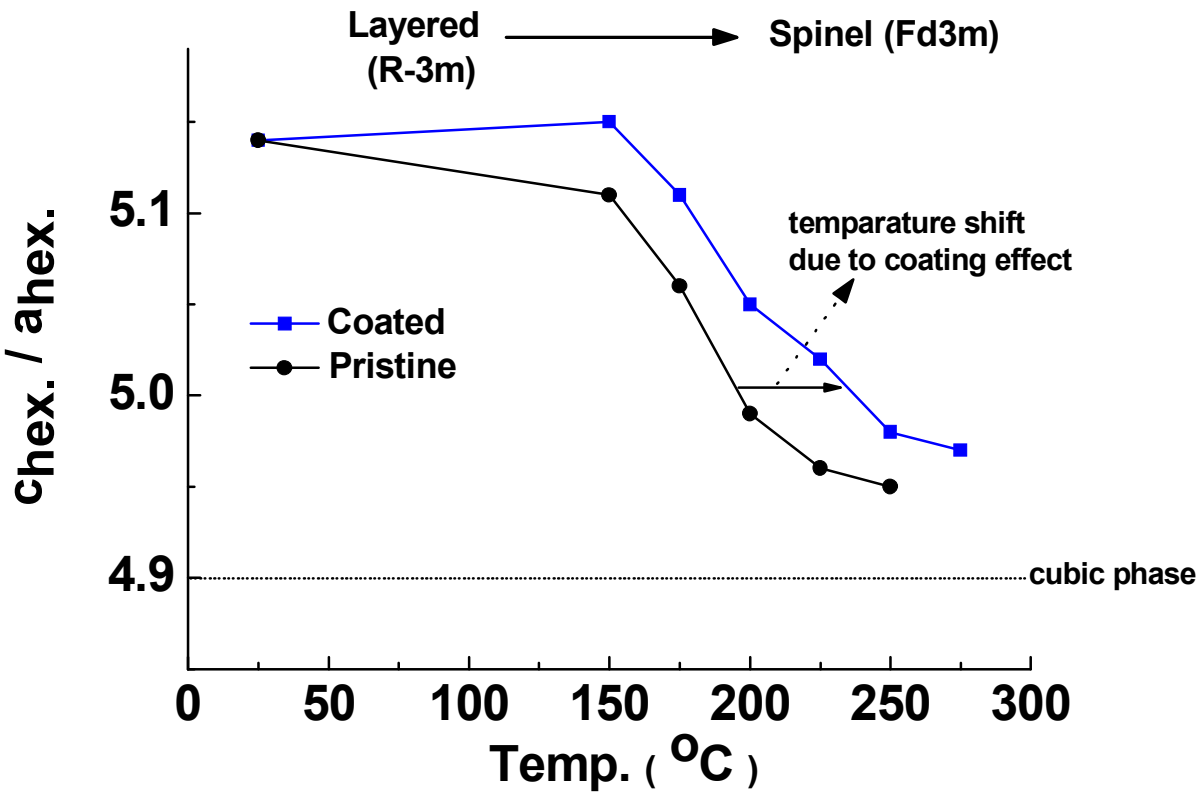


**Figure 20**. Evolution of the $c_{hex}/ a_{hex}$ ratio as a function of temperature for pristine and coated cathodes.

# V. CONCLUSIONS

Nanoscale $SiP_2O_7$ coating onto $Ni_{0.5}Co_{0.2}Mn_{0.3}(OH)_2$ precursors followed by annealing with a Li source led to the formation of an amorphous $Li_\delta P_yO_z$-like thin coating layer on the $LiNi_{0.5}Co_{0.2}Mn_{0.3}O_2$ particles with doped with P and Si ions. The amorphous coating layer significantly improved the rate capability, even at a 7C rate cycling, resulting in 83 $mAhg^{-1}$, while the pristine cathode showed a result of 0 $mAhg^{-1}$. Moreover, the evolved amount of oxygen upon an increase in the cathode at 4.5V was reduced by 79% compared to the pristine sample. Overall, this coating method is also applicable to other bulk cathodes, such as $LiMn_2O_4$ and $LiCoO_2$ which need to improve electrochemical properties both at room and elevated temperatures.

# VI. Acknowledgements

This work was supported by the grant from the Technology Innovation Program of the Ministry of Knowledge Economy of Korea (Project No. 10032319). This research was also supported by the MKE (The Ministry of Knowledge Economy), Korea, under the ITRC(Information Technology Research Center) support program supervised by the NIPA(National IT Industry Promotion Agency) (NIPA-2011-C1090-1100-0002)

# Ⅶ. REFERENCES


1. ROSSEN, E., JONES, C. D. W. & DAHN, J. R. 1992. STRUCTURE AND ELECTROCHEMISTRY OF LIXMNYNI1-YO2. *Solid State Ionics,* 57**,** 311-318.
2. OMANDA, H., BROUSSE, T., MARHIC, C. & SCHLEICH, D. M. 2004. Improvement of the thermal stability of LiNi0.8Co0.2O2 cathode by a SiOx protective coating. *Journal of the Electrochemical Society,* 151**,** A922-A929.
3. CHO, J. 2001. Stabilization of spinel-like phase transformation of o-LiMnO2 during 55 degrees C cycling by sol-gel coating of CoO. *Chemistry of Materials,* 13**,** 4537-4541.
4. YOSHIO, M., NOGUCHI, H., ITOH, J., OKADA, M. & MOURI, T. 2000. Preparation and properties of LiCoyMnxNi1-x-yO2 as a cathode for lithium ion batteries. *Journal of Power Sources,* 90**,** 176-181.
5. YABUUCHI, N. & OHZUKU, T. 2003. Novel lithium insertion material of LiCo1/3Ni1/3Mn1/3O2 for advanced lithium-ion batteries. *Journal of Power Sources,* 119**,** 171-174.
6. CHOI, J. & MANTHIRAM, A. 2005. Investigation of the irreversible capacity loss in the layered LiNi1/3Mn1/3Co1/3O2 cathodes. *Electrochemical and Solid State Letters,* 8**,** C102-C105.
7. SHAJU, K. M., RAO, G. V. S. & CHOWDARI, B. V. R. 2004. Influence of Li-ion kinetics in the cathodic performance of layered Li(Ni1/3Co1/3Mn1/3)O-2. *Journal of the Electrochemical Society,* 151**,** A1324-A1332.
8. LEE, H., KIM, M. G. & CHO, J. 2007. Olivine LiCoPO4 phase grown LiCoO2 cathode material for high density Li batteries. *Electrochemistry Communications,* 9**,** 149-154.
9. EOM, J. & CHO, J. 2008. M-3(PO4)(2)-nanoparticle-coated LiCoO2 vs LiCo0.96M0.04O2 (M = Mg and Zn) on electrochemical and storage characteristics. *Journal of the Electrochemical Society,* 155**,** A201-A205.
10. CHO, Y., LEE, Y. S., PARK, S. A., LEE, Y. & CHO, J. 2010. LiNi(0.8)Co(0.15)Al(0.05)O(2) cathode materials prepared by TiO(2) nanoparticle coatings on Ni(0.8)Co(0.15)Al(0.05)(OH)(2) Precursors. *Electrochimica Acta,* 56**,** 333-339.
11. KIM, M. G. & CHO, J. 2009. Reversible and High-Capacity Nanostructured Electrode Materials for Li-Ion Batteries. *Advanced Functional Materials,* 19**,** 1497-1514.
12. CHO, Y. & CHO, J. 2010. Significant Improvement of LiNi(0.8)Co(0.15)Al(0.05)O(2) Cathodes at 60 degrees C by SiO(2) Dry Coating for Li-Ion Batteries. *Journal of the Electrochemical Society,* 157**,** A625-A629.
13. SONG, H. K., LEE, K. T., KIM, M. G., NAZAR, L. F. & CHO, J. 2010. Recent Progress in Nanostructured Cathode Materials for Lithium Secondary Batteries. *Advanced Functional Materials,* 20**,** 3818-3834.
14. ZHOU, F., ZHAO, X. M., LU, Z. H., JIANG, J. W. & DAHN, J. R. 2008. The effect of Al substitution on the reactivity of delithiated LiNi((0.5-z))Mn((0.5-z))A1(2z)O(2) with nonaqueous electrolyte. *Electrochemical and Solid State Letters,* 11**,** A155-A157.
15. CHO, J., KIM, T. J., KIM, J., NOH, M. & PARK, B. 2004. Synthesis, thermal, and electrochemical properties of AlPO4-coated LiNi0.8Co0.1Mn0.1O2 cathode materials for a Li-ion cell. *Journal of the Electrochemical Society,* 151**,** A1899-A1904.
16. BELHAROUAK, I., LU, W. Q., VISSERS, D. & AMINE, K. 2006. Safety characteristics of Li(Ni0.8Co0.15Al0.05)O-2 and Li(Ni1/3CO1/3Mn1/3)O-2. *Electrochemistry Communications,* 8**,** 329-335.
17. JO, M., JEONG, S. & CHO, J. 2010. High power LiCoO(2) cathode materials with ultra energy density for Li-ion cells. *Electrochemistry Communications,* 12**,** 992-995.
18. ARAI, H., OKADA, S., SAKURAI, Y. & YAMAKI, J. 1998. Thermal behavior of Li1-yNiO2 and the decomposition mechanism. *Solid State Ionics,* 109**,** 295-302.
19. LIAO, P. Y., DUH, J. G. & SHEEN, S. R. 2005. Effect of Mn content on the microstructure and electrochemical performance of LiNi0.75-xCo0.25MnxO2 cathode materials. *Journal of the Electrochemical Society,* 152**,** A1695-A1700.
20. LI, J. G., WANG, L., ZHANG, Q. & HE, X. M. 2009. Synthesis and characterization of LiNi(0.6)Mn(0.4-x)Co(x)O(2) as cathode materials for Li-ion batteries. *Journal of Power Sources,* 189**,** 28-33.
21. SUN, Y. K., MYUNG, S. T., PARK, B. C., PRAKASH, J., BELHAROUAK, I. & AMINE, K. 2009. High-energy cathode material for long-life and safe lithium batteries. *Nature Materials,* 8**,** 320-324.
22. CHO, Y., LEE, S., LEE, Y., HONG, T. & CHO, J. 2011. Spinel-Layered Core-Shell Cathode Materials for Li-Ion Batteries. *Advanced Energy Materials,* 1**,** 821-828.
23. BANG, H., KIM, D. H., BAE, Y. C., PRAKASH, J. & SUN, Y. K. 2008. Effects of Metal Ions on the

Structural and Thermal Stabilities of Li Ni(1-x-y)Co(x)Mn(y) O(2) (x plus y <= 0.5) studied by in situ high temperature XRD. *Journal of the Electrochemical Society,* 155**,** A952-A958.
24. EOM, J., KIM, M. G. & CHO, J. 2008. Storage characteristics of LiNi0.8Co0.1+xMn0.1-xO2 (x=0, 0.03, and 0.06) cathode materials for lithium batteries. *Journal of the Electrochemical Society,* 155**,** A239-A245.
25. GABANO, J.-P. 1983. Lithium batteries.
26. NAZRI, G.-A. A. P. G. 2009. Lithium batteries: Science and Technology. *Springer*.
27. BESENHARD, J. O. 1999. Handbook of Battery Materials. *Wiley-VCH*.
28. BROUSSLEY, M. A. P., G 2007. Industrial Applications of Batteries. *Elsevier*.
29. ABRAHAM, K. M., PASQUARIELLO, D. M. & SCHWARTZ, D. A. 1989. PRACTICAL RECHARGEABLE LITHIUM BATTERIES. *Journal of Power Sources,* 26**,** 247-255.
30. BRANDT, K. & LAMAN, F. C. 1989. REPRODUCIBILITY AND RELIABILITY OF RECHARGEABLE LITHIUM MOLYBDENUM-DISULFIDE BATTERIES. *Journal of Power Sources,* 25**,** 265-276.
31. DAN, P., MENGERITSKI, E., GERONOV, Y., AURBACH, D. & WEISMAN, I. 1995. PERFORMANCES AND SAFETY BEHAVIOR OF RECHARGEABLE AA-SIZE LI/LIXMNO2 CELL(R). *Journal of Power Sources,* 54**,** 143-145.
32. MENGERITSKY, E., DAN, P., WEISSMAN, I., ZABAN, A. & AURBACH, D. 1996. Safety and performance of Tadiran TLR-7103 rechargeable batteries. *Journal of the Electrochemical Society,* 143**,** 2110-2116.
33. AURBACH, D. 2000. Review of selected electrode-solution interactions which determine the performance of Li and Li ion batteries. *Journal of Power Sources,* 89**,** 206-218.
34. SCROSATI, B. 1993. Electrochemistry of Novel Materials. *VCH Publishers*.
35. WHITTINGHAM, M. S. 2004. Lithium batteries and cathode materials. *Chemical Reviews,* 104**,** 4271-4301.
36. KAMALI, A. R. & FRAY, D. J. 2010. Review on Carbon and Silicon Based Materials as Anode Materials for Lithium Ion Batteries. *Journal of New Materials for Electrochemical Systems,* 13**,** 147-160.
37. VERMA, P., MAIRE, P. & NOVAK, P. 2010. A review of the features and analyses of the solid electrolyte interphase in Li-ion batteries. *Electrochimica Acta,* 55**,** 6332-6341.
38. DAHN, J. R., VONSACKEN, U. & MICHAL, C. A. 1990. STRUCTURE AND ELECTROCHEMISTRY OF LI1+/-YNIO2 AND A NEW LI2NIO2 PHASE WITH THE NI(OH)2 STRUCTURE. *Solid State Ionics,* 44**,** 87-97.
39. ROUGIER, A., SAADOUNE, I., GRAVEREAU, P., WILLMANN, P. & DELMAS, C. 1996. Effect of cobalt substitution on cationic distribution in LiNi1-yCoyO2 electrode materials. *Solid State Ionics,* 90**,** 83-90.
40. SAADOUNE, I., MENETRIER, M. & DELMAS, C. 1997. Redox processes in LixNi1-yCoyO2 cobalt-rich phases. *Journal of Materials Chemistry,* 7**,** 2505-2511.
41. SAADOUNE, I. & DELMAS, C. 1998. On the LixNi0.8Co0.2O2 system. *Journal of Solid State Chemistry,* 136**,** 8-15.
42. SAADOUNE, I. & DELMAS, C. 1996. LiNi1-yCoyO2 positive electrode materials: Relationships between the structure, physical properties and electrochemical behaviour. *Journal of Materials Chemistry,* 6**,** 193-199.
43. PRADO, G., FOURNES, L. & DELMAS, C. 2001. On the LixNi0.70Fe0.15Co0.15O2 system: An X-ray diffraction and Mossbauer study. *Journal of Solid State Chemistry,* 159**,** 103-112.
44. PRADO, G., ROUGIER, A., FOURNES, L. & DELMAS, C. 2000. Electrochemical behavior of iron-substituted lithium nickelate. *Journal of the Electrochemical Society,* 147**,** 2880-2887.
45. KANNO, R., SHIRANE, T., INABA, Y. & KAWAMOTO, Y. 1997. Synthesis and electrochemical properties of lithium iron oxides with layer-related structures. *Journal of Power Sources,* 68**,** 145-152.
46. POUILLERIE, C., PERTON, F., BIENSAN, P., PERES, J. P., BROUSSELY, M. & DELMAS, C. 2001. Effect of magnesium substitution on the cycling behavior of lithium nickel cobalt oxide. *Journal of Power Sources,* 96**,** 293-302.
47. POUILLERIE, C., CROGUENNEC, L. & DELMAS, C. 2000. The LixNi1-yMgyO2 (y=0.05, 0.10) system: structural modifications observed upon cycling. *Solid State Ionics,* 132**,** 15-29.
48. NAKAI, I. & NAKAGOME, T. 1998. In situ transmission X-ray absorption fine structure analysis of the Li deintercalation process in Li(Ni0.5Co0.5)O-2. *Electrochemical and Solid State Letters,* 1**,** 259-261.
49. OHZUKU, T. & MAKIMURA, Y. 2001. Layered lithium insertion material of LiCo1/3Ni1/3Mn1/3O2 for lithium-ion batteries. *Chemistry Letters***,** 642-643.

50. LU, Z. H., MACNEIL, D. D. & DAHN, J. R. 2001. Layered Li NixCo1-2xMnx O-2 cathode materials for lithium-ion batteries. *Electrochemical and Solid State Letters,* 4**,** A200-A203.
51. PARK, S. H., YOON, C. S., KANG, S. G., KIM, H. S., MOON, S. I. & SUN, Y. K. 2004. Synthesis and structural characterization of layered Li Ni1/3Co1/3Mn1/3 O-2 cathode materials by ultrasonic spray pyrolysis method. *Electrochimica Acta,* 49**,** 557-563.
52. LIU, Z. L., YU, A. S. & LEE, J. Y. 1999. Synthesis and characterization of LiNi1-x-yCoxMnyO2 as the cathode materials of secondary lithium batteries. *Journal of Power Sources,* 81**,** 416-419.
53. SON, J. T. & CAIRNS, E. J. 2006. Preparation and characterization of Li-1.05 Ni0.35Co025Mn0.4 O-2 as a cathode material for rechargeable lithium cells. *Electrochemical and Solid State Letters,* 9**,** A27-A30.
54. KIM, M. H., SHIN, H. S., SHIN, D. & SUN, Y. K. 2006. Synthesis and electrochemical properties of Li Ni0.8Co0.1Mn0.1 O-2 and Li Ni0.8Co0.2 O-2 via co-precipitation. *Journal of Power Sources,* 159**,** 1328-1333.
55. LEE, K. S., MYUNG, S. T., AMINE, K., YASHIRO, H. & SUN, Y. K. 2007. Structural and electrochemical properties of layered Li Ni1-2xCoxMnx O-2 (x=0.1-0.3) positive electrode materials for Li-ion batteries. *Journal of the Electrochemical Society,* 154**,** A971-A977.
56. DELMAS, C., SAADOUNE, I. & ROUGIER, A. 1993. THE CYCLING PROPERTIES OF THE LIXNI1-YCOYO2 ELECTRODE. *Journal of Power Sources,* 44**,** 595-602.
57. CHO, J., KIM, G. & LIM, H. S. 1999. Effect of preparation methods of LiNi1-xCoxO2 cathode materials on their chemical structure and electrode performance. *Journal of the Electrochemical Society,* 146**,** 3571-3576.
58. ARAI, H., OKADA, S., SAKURAI, Y. & YAMAKI, J. 1997. Electrochemical and thermal behavior of LiNi1-zMzO2 (M = Co, Mn, Ti). *Journal of the Electrochemical Society,* 144**,** 3117-3125.
59. SHIM, J., KOSTECKI, R., RICHARDSON, T., SONG, X. & STRIEBEL, K. A. 2002. Electrochemical analysis for cycle performance and capacity fading of a lithium-ion battery cycled at elevated temperature. *Journal of Power Sources,* 112**,** 222-230.
60. BANG, H. J., JOACHIN, H., YANG, H., AMINE, K. & PRAKASH, J. 2006. Contribution of the structural changes of LiNi0.8Co0.15Al0.05O2 cathodes on the exothermic reactions in Li-ion cells. *Journal of the Electrochemical Society,* 153**,** A731-A737.
61. ZHONG, Q. M. & VONSACKEN, U. 1995. CRYSTAL-STRUCTURES AND ELECTROCHEMICAL PROPERTIES OF LIALYNI1-YO2 SOLID-SOLUTION. *Journal of Power Sources,* 54**,** 221-223.
62. GAO, Y. A., YAKOVLEVA, M. V. & EBNER, W. B. 1998. Novel LiNi1-xTix/2Mgx/2O2 compounds as cathode materials for safer lithium-ion batteries. *Electrochemical and Solid State Letters,* 1**,** 117-119.
63. DELMAS, C., MENETRIER, M., CROGUENNEC, L., SAADOUNE, I., ROUGIER, A., POUILLERIE, C., PRADO, G., GRUNE, M. & FOURNES, L. 1999. An overview of the Li(Ni,M)O-2 systems: syntheses, structures and properties. *Electrochimica Acta,* 45**,** 243-253.
64. CHEBIAM, R. V., PRADO, F. & MANTHIRAM, A. 2001. Structural instability of delithiated Li1-xNi1-yCoyO2 cathodes. *Journal of the Electrochemical Society,* 148**,** A49-A53.
65. ZENG, D. L., CABANA, J., BREGER, J. L., YOON, W. S. & GREY, C. P. 2007. Cation ordering in Li NixMnxCo(1-2x) O-2-layered cathode materials: A nuclear magnetic resonance (NMR), pair distribution function, X-ray absorption spectroscopy, and electrochemical study. *Chemistry of Materials,* 19**,** 6277-6289.
66. CHO, J. P., KIM, T. J., KIM, Y. J. & PARK, B. 2001. Complete blocking of Mn3+ ion dissolution from a LiMn2O4 spinel intercalation compound by Co3O4 coating. *Chemical Communications***,** 1074-1075.
67. KIM, M. G., SHIN, H. J., KIM, J. H., PARK, S. H. & SUN, Y. K. 2005. XAS investigation of inhomogeneous metal-oxygen bond covalency in bulk and surface for charge compensation in li-ion battery cathode Li Ni1/3Co1/3Mn1/3 O-2 material. *Journal of the Electrochemical Society,* 152**,** A1320-A1328.
68. THACKERAY, M. M. 1997. Manganese oxides for lithium batteries. *Progress in Solid State Chemistry,* 25**,** 1-71.
69. BLYR, A., SIGALA, C., AMATUCCI, G., GUYOMARD, D., CHABRE, Y. & TARASCON, J. M. 1998. Self-discharge of LiMn2O4/C Li-ion cells in their discharged state - Understanding by means of three-electrode measurements. *Journal of the Electrochemical Society,* 145**,** 194-209.
70. GUMMOW, R. J., DEKOCK, A. & THACKERAY, M. M. 1994. IMPROVED CAPACITY RETENTION IN RECHARGEABLE 4V LITHIUM LITHIUM MANGANESE OXIDE (SPINEL) CELLS. *Solid State Ionics,* 69**,** 59-67.
71. XIA, Y. Y., M 2004. Lithium Batteries Science and Technology (Eds: G.-A. Nazri, G. Pistoia, G.-A.).

p. 361.
72. WAKIHARA, M. L., G. IKUTA, H. 1998. Lithium Batteries—Fundamentals and Performance (Eds: M. Wakihara, O. Yamamoto). *Kodansha, Japan, and Wiley-VCH, Germany* p. 26.
73. AMATUCCI, G. G. T., J.-M. 1996. *U.S. Patent # 5705291*.
74. CHO, J. P. & KIM, G. 1999. Enhancement of thermal stability of LiCoO2 by LiMn2O4 coating. *Electrochemical and Solid State Letters,* 2**,** 253-255.
75. CHO, J., KIM, G. B., LIM, H. S., KIM, C. S. & YOO, S. I. 1999. Improvement of structural stability of LiMn2O4 cathode material on 55 degrees C cycling by sol-gel coating of LiCoO2. *Electrochemical and Solid State Letters,* 2**,** 607-609.
76. CHO, J., KIM, Y. J. & PARK, B. 2000. Novel LiCoO2 cathode material with Al2O3 coating for a Li ion cell. *Chemistry of Materials,* 12**,** 3788-3791.
77. SUN, Y. K., HONG, K. J., PRAKASH, J. & AMINE, K. 2002. Electrochemical performance of nano-sized ZnO-coated LiNi0.5Mn1.5O4 spinel as 5 V materials at elevated temperatures. *Electrochemistry Communications,* 4**,** 344-348.
78. SUN, Y. K., LEE, Y. S., YOSHIO, M. & AMINE, K. 2002. Synthesis and electrochemical properties of ZnO-coated LiNi0.5Mn1.5O4 spinel as 5 V cathode material for lithium secondary batteries. *Electrochemical and Solid State Letters,* 5**,** A99-A102.
79. KWEON, H. J. & PARK, D. G. 2000. Surface modification of LiSr0.002Ni0.9Co0.1O2 by overcoating with a magnesium oxide. *Electrochemical and Solid State Letters,* 3**,** 128-130.
80. CHOWDARI, B. V. R., RAO, G. V. S. & CHOW, S. Y. 2002. Cathodic performance of anatase (TiO2)-coated Li (Ni0.8Co0.2)O-2. *Journal of Solid State Electrochemistry,* 6**,** 565-567.
81. KANNAN, A. M. & MANTHIRAM, A. 2002. Surface/Chemically modified LiMn2O4 cathodes for lithium-ion batteries. *Electrochemical and Solid State Letters,* 5**,** A167-A169.
82. ZHANG, Z. R., LIU, H. S., GONG, Z. L. & YANG, Y. 2004. Comparison of electrochemical and surface properties of bare and TiO2-coated LiNi0.8Co0.2O2 electrodes. *Journal of the Electrochemical Society,* 151**,** A599-A603.
83. THACKERAY, M. M., JOHNSON, C. S., KIM, J. S., LAUZZE, K. C., VAUGHEY, J. T., DIETZ, N., ABRAHAM, D., HACKNEY, S. A., ZELTNER, W. & ANDERSON, M. A. 2003. ZrO2- and Li2ZrO3-stabilized spinel and layered electrodes for lithium batteries. *Electrochemistry Communications,* 5**,** 752-758.
84. PASQUALI, M. P., S. PISTOIA, G 2003. Science and Technology of lithium batteries (Chapter 11) (Eds: G.-H. Nazari, G. Pistoia). *Kluwer Academic Publishers*.
85. SUN, Y. K., HONG, K. J. & PRAKASH, J. 2003. The effect of ZnO coating on electrochemical cycling behavior of spinel LiMn2O4 cathode materials at elevated temperature. *Journal of the Electrochemical Society,* 150**,** A970-A972.
86. KIM, Y. J., CHO, J. P., KIM, T. J. & PARK, B. 2003. Suppression of cobalt dissolution from the LiCoO2 cathodes with various metal-oxide coatings. *Journal of the Electrochemical Society,* 150**,** A1723-A1725.
87. LEE, H., KIM, Y., HONG, Y. S., KIM, M. G., SHIN, N. S. & CHO, J. 2006. Structural characterization of the surface-modified LixNi0.9Co0.1O2 cathode materials by MPO4 coating (M = Al, Ce, SrH, and Fe) for Li-ion cells. *Journal of the Electrochemical Society,* 153**,** A781-A786.
88. KIM, J., NOH, M., CHO, J., KIM, H. & KIM, K. B. 2005. Controlled nanoparticle metal phosphates (metal = Al, Fe, Ce, and Sr) coatings on LiCoO2 cathode materials. *Journal of the Electrochemical Society,* 152**,** A1142-A1148.
89. KWON, Y., PARK, G. S. & CHO, J. H. 2007. Synthesis and electrochemical properties of lithium-electroactive surface-stabilized silicon quantum dots. *Electrochimica Acta,* 52**,** 4663-4668.
90. ZIOLKOWSKI, J. 1985. NEW RELATION BETWEEN IONIC-RADII, BOND LENGTH, AND BOND STRENGTH. *Journal of Solid State Chemistry,* 57**,** 269-290.
91. ITOU, Y. & UKYO, Y. 2005. Performance of LiNiCoO2 materials for advanced lithium-ion batteries. *Journal of Power Sources,* 146**,** 39-44.
92. KANG, B. & CEDER, G. 2009. Battery materials for ultrafast charging and discharging. *Nature,* 458**,** 190-193.
93. ADAMS, S. 2010. Lithium ion pathways in LiFePO(4) and related olivines. *Journal of Solid State Electrochemistry,* 14**,** 1787-1792.
94. MAIER, J. 2009. Thermodynamics of Nanosystems with a Special View to Charge Carriers. *Advanced Materials,* 21**,** 2571-2585.
95. LEE, K. T. & CHO, J. 2011. Roles of nanosize in lithium reactive nanomaterials for lithium ion batteries. *Nano Today,* 6**,** 28-41.
96. DELMAS, C., MACCARIO, M., CROGUENNEC, L., LE CRAS, F. & WEILL, F. 2008. Lithium

deintercalation in LiFePO(4) nanoparticles via a domino-cascade model. *Nature Materials,* 7**,** 665-671.
97. ANDERSSON, A. M., ABRAHAM, D. P., HAASCH, R., MACLAREN, S., LIU, J. & AMINE, K. 2002. Surface characterization of electrodes from high power lithium-ion batteries. *Journal of the Electrochemical Society,* 149**,** A1358-A1369.
98. MARTHA, S. K., MARKEVICH, E., BURGEL, V., SALITRA, G., ZINIGRAD, E., MARKOVSKY, B., SCLAR, H., PRAMOVICH, Z., HEIK, O., AURBACH, D., EXNAR, I., BUQA, H., DREZEN, T., SEMRAU, G., SCHMIDT, M., KOVACHEVA, D. & SALIYSKI, N. 2009. A short review on surface chemical aspects of Li batteries: A key for a good performance. *Journal of Power Sources,* 189**,** 288-296.
99. LIU, H. S., ZHANG, Z. R., GONG, Z. L. & YANG, Y. 2004. Origin of deterioration for LiNiO2 cathode material during storage in air. *Electrochemical and Solid State Letters,* 7**,** A190-A193.
100. LI, J., ZHENG, J. M. & YANG, Y. 2007. Studies on storage characteristics of LiNi0.4Co0.2Mn0.4O2 as cathode materials in lithium-ion batteries. *Journal of the Electrochemical Society,* 154**,** A427-A432.
101. KIM, J., NOH, M. & CHO, J. 2006. Improvement of 12 V overcharge behavior of LiCoO2 cathode material by LiNi0.8Co0.1Mn0.1O2 addition in a Li-ion cell. *Journal of Power Sources,* 153**,** 345-349.
102. MALEKI, H., DENG, G. P., KERZHNER-HALLER, I., ANANI, A. & HOWARD, J. N. 2000. Thermal stability studies of binder materials in anodes for lithium-ion batteries. *Journal of the Electrochemical Society,* 147**,** 4470-4475.
103. GUILMARD, M., CROGUENNEC, L., DENUX, D. & DELMAS, C. 2003. Thermal stability of lithium nickel oxide derivatives. Part I: LixNi1.02O2 and LixNi0.89Al0.16O2 (x = 0.50 and 0.30). *Chemistry of Materials,* 15**,** 4476-4483.